Advanced Robotics

ISSN: 0169-1864 (Print) 1568-5535 (Online) Journal homepage: https://www.tandfonline.com/loi/tadr20

Neural adaptive PID formation control of car-like mobile robots without velocity measurements

Khoshnam Shojaei

To cite this article: Khoshnam Shojaei (2017) Neural adaptive PID formation control of car-like mobile robots without velocity measurements, Advanced Robotics, 31:18, 947-964, DOI: 10.1080/01691864.2017.1368413

To link to this article: https://doi.org/10.1080/01691864.2017.1368413

ADVANCED ROBOTICS, 2017
VOL. 31, NO. 18, 947–964
https://doi.org/10.1080/01691864.2017.1368413

RSJ Taylor & Francis
Taylor & Francis Group

FULL PAPER

Neural adaptive PID formation control of car-like mobile robots without velocity measurements

Khoshnam Shojaei

Department of Electrical Engineering, Najafabad Branch, Islamic Azad University, Najafabad, Iran

ABSTRACT

A virtual leader–follower formation control of a group of car-like mobile robots is addressed in this paper. First, the kinematic and dynamic models of car-like robots are transformed into a second-order leader–follower formation model which inherits all structural properties of the robot dynamic model. Then, a new observer-based proportional–integral-derivative formation controller is proposed to force that all robots construct a desired formation with respect to a predefined virtual leader. To improve the formation tracking and observation performance, the integral action is incorporated into the design of the observer–controller scheme. Adaptive robust and neural network techniques are also employed to compensate uncertain parameters, unmodeled dynamics, and external disturbances. Lyapunov's direct method is utilized to show that the formation tracking and observation errors are semi-globally uniformly ultimately bounded. Then, the proposed controller is extended to the leader–follower formation of a team of tractor–trailer systems. Finally, simulation results illustrate the efficiency of the proposed controller.

ARTICLE HISTORY
Received 22 March 2016
Revised 5 August 2016 and 19 May 2017
Accepted 9 August 2017

KEYWORDS
Adaptive control; car-like mobile robots; leader–follower formation; output-feedback PID control; neural networks

1. Introduction

The cooperative and formation control of multiple agents has attracted a lot of attention among control and robotic researchers over recent years due to the robustness against individual failures, redundancy, and efficiency of agents teamwork with respect to a single agent. Potential applications of robots formation in automation systems include military cooperation, surveillance, load carriage, crop harvesting, material collecting, delivery systems, autonomous exploration, reconnaissance, coverage, transportation, and rescue operations. There exist three well-known methodologies for the formation control of mobile robots including behavioral-based [1,2], virtual structure [3,4], and leader–follower [5,6]. According to the literature [1–20], the most popular approach is the leader–follower formation system due to its simplicity, reliability, and scalability [5–7] that all followers maintain desired ranges and bearing angles from a predefined leader. Recently, various aspects of mobile robots formations have been addressed in the literature. As some examples, Dierks et al. [8] have proposed a neural network-based optimal formation controller for wheeled mobile robots with reduced information exchange. A leader–follower formation controller has been proposed based on a bioinspired neurodynamic-based approach for nonholonomic mobile robots in [9]. An adaptive leader–follower formation controller has been designed in [10] for nonholonomic mobile robots using active vision. In [11], the adaptive formation control of multi-robotic vehicles has been addressed using the backstepping technique and rigid graph theory. Distributed formation tracking of networked mobile robots under unknown slippage effects has been addressed in [12].

Based on the presented literature review [1–20], most of previous formation controllers have been proposed for unicycle-type and differentially driven wheeled mobile robots [1–16] and a few works pay attention to the formation control of car-like mobile robots (CLMRs) [17–19]. Unfortunately, previously proposed controllers including [1–16] are not applicable to the formation control of CLMRs. In [17], a decentralized control strategy is proposed for CLMRs formation based on the leader–follower approach. Moreover, formation tracking controllers have been proposed for CLMRs using the backstepping approach in [18,19]. However, a main shortcoming in previous works is that their proposed controllers cannot be implemented without velocity measurements for feedback. In practice, velocity signals are not easily measurable due to communication delays and noise contamination.

CONTACT Khoshnam Shojaei shojaei@pel.iaun.ac.ir

Moreover, velocity sensors increase the weight and the cost of agents. In consequence, the development of a formation controller which only needs position measurements is of great importance. One approach to determine the velocity signal is the use of first-order numerical differentiation of the position signal. The simplicity of this method is especially useful for real implementations. According to [21] and references therein, this technique suffers from following shortcomings: (1) such an approximation degrades the controller performance in low and high velocities; (2) quantization effects, that are inherently available in this approach, may generate undesired oscillations in the tracking response; and (3) even if the approximation errors are compensated as a part of uncertainties, there is not any theoretical justification for this ad hoc solution, that is, closed-loop stability properties are not guaranteed according to [21]. Therefore, the design of observer-based controllers is widely recommended to obviate the need for velocity measurements. Since the separation principle does not hold for nonlinear systems, the design of observer-based controllers is a challenging task. In addition, nonholonomic constraints of mobile robots make this problem more demanding. The problem is even more troublesome in the presence of unmodeled dynamics and external disturbances. To overcome this problem, some researchers have proposed observer-based formation controllers in [13–16] which are only applicable to differential drive mobile robots. Besides, presented observers in such works extremely depend on the approximation of system dynamics.

In this work, an observer-based proportional–integral-derivative (PID) formation controller is proposed for a team of CLMRs. An adaptive *radial basis function neural network* (RBFNN) is utilized to approximate uncertain nonlinearities of the formation model. A Lyapunov-based stability analysis shows that the tracking and states estimation errors are semi-globally uniformly ultimately bounded (SGUUB) for all agents. Compared with the existing results [1–20], novelties and main contributions of this paper are expressed as follows:

(1) A new observer-based PID leader–follower formation control scheme is proposed for a high-performance formation maneuvring of CLMRs which is not addressed in the literature to the best of author's knowledge. The proposed controller takes the advantage of a projection-type adaptive neural network technique to compensate uncertain dynamics of CLMRs.
(2) A new second-order leader-following formation model is proposed for CLMRs for the first time which inherits all structural properties of the robot dynamics. This formation model effectively helps us design an observer-based PID controller.
(3) In contrast to the most of previous output-feedback formation controllers [13–16], the proposed observer does not need to know the exact kinematic and dynamic models of robots. Moreover, an integral action is incorporated into the design of the observer–controller scheme to improve the formation tracking and observation performance.
(4) The proposed leader–follower output-feedback (OFB) formation tracking controller is applied to a team of tractor–trailer wheeled mobile robots (TTWMRs) which is not sufficiently addressed in the literature.

This brief is organized as follows. Section 2 presents the problem statement. Section 3 introduces an observer-based PID formation controller and its stability analysis. In Section 4, the proposed approach is extended to the formation control of tractor–trailer mobile robots. Section 5 gives numerical simulation results. Finally, Section 6 concludes this paper.

2. Problem formulation

2.1. Notations

Throughout this paper, $\|x\| := \sqrt{x^T x}$ is used to show Euclidean norm of a vector $x \in \Re^n$, while the norm of a matrix A is defined by the induced norm $\|A\| := \sqrt{\lambda_{\max}(A^T A)}$, and Frobenius norm, i.e. $\|A\|_F := \sqrt{\mathrm{tr}\{A^T A\}}$, where $\mathrm{tr}\{\bullet\}$ is the trace operator. The matrix I_n represents n-dimensional identity matrix. The term $\lambda_{\max}(\bullet)$ ($\lambda_{\min}(\bullet)$) shows the largest (smallest) eigenvalue of a matrix. $\{\alpha_i\}_{i=1}^n := \{\alpha_1, \alpha_2, \ldots, \alpha_n\}$ denotes a set of α_i, $i = 1, \ldots, n$. In addition, $\Re^+$ denotes the set of positive real numbers.

2.2. Kinematic and dynamic models

Consider a team of N car-like wheeled mobile robots which are subjected to nonholonomic constraints. The dynamic equation of ith CLMR is represented by the following Euler–Lagrange formulation [22–24]:

$$\begin{cases} M_{1i}(\eta_i)\ddot{\eta}_i + C_{1i}(\eta_i, \dot{\eta}_i)\dot{\eta}_i + D_{1i}\dot{\eta}_i + \tau_{d1i}(t) = B_{1i}(\eta_i)\tau_i - A_i^T(\eta_i)\lambda_i, \\ A_i(\eta_i)\dot{\eta}_i = 0, \quad i = 1, 2, \ldots, N \end{cases} \tag{1}$$

where $\eta_i = [x_i, y_i, \psi_i, \gamma_i]^T$ is a vector of generalized coordinates, x_i, y_i, and ψ_i denote the robot position and orientation, respectively, γ_i is the steering angle of the robot, $\tau_i \in \Re^2$ represents a vector of actuators inputs,

$M_{1i}(\eta_i) \in \mathfrak{R}^{4\times4}$ is a symmetric positive-definite inertia matrix, $C_{1i}(\eta_i, \dot{\eta}_i) \in \mathfrak{R}^{4\times4}$ is the centripetal and Coriolis matrix, $D_{1i} \in \mathfrak{R}^{4\times4}$ denotes the damping matrix, $\tau_{d1i}(t) \in \mathfrak{R}^4$ denotes a time-varying disturbance vector, $B_{1i}(\eta_i) \in \mathfrak{R}^{4\times2}$ is the input transformation matrix, $A_i(\eta_i) \in \mathfrak{R}^{2\times4}$ is a full-rank matrix, $\lambda_i \in \mathfrak{R}^2$ denotes a vector of Lagrange multipliers which show constraint forces and $A_i(\eta_i)\dot{\eta}_i = 0$ represents nonholonomic constraints.

From a review of [22,25], let $S_i(\eta_i) = [s_{1i}(\eta_i), s_{2i}(\eta_i)]^T$ be a full-rank matrix that is made up of a set of smooth and linearly independent vector fields, $s_{1i}(\eta_i) = [\cos\psi_i, \sin\psi_i, 1/a_i \tan\gamma_i, 0]^T$ and $s_{2i}(\eta_i) = [0, 0, 0, 1]^T$, in the null space of $A_i(\eta_i)$ i.e. $A_i(\eta_i)S_i(\eta_i) = 0$. By considering $A_i(\eta_i)\dot{\eta}_i = 0$, one may find a vector of pseudo-velocities of the system as $v_i(t) = [v_i(t), \omega_i(t)]^T$, where $v_i(t)$ and $\omega_i(t)$ are linear and steering velocities, respectively, such that

$$\dot{\eta}_i(t) = S_i(\eta_i)v_i(t) = s_{1i}(\eta_i)v_i(t) + s_{2i}(\eta_i)\omega_i(t). \quad (2)$$

Differentiating (2) yields $\ddot{\eta}_i = \dot{S}_i(\eta_i)v_i + S_i(\eta_i)\dot{v}_i$ which together with (2) are substituted into (1) and the result is multiplied by $S_i^T(\eta_i)$ to give the following dynamic equation:

$$M_{2i}(\eta_i)\dot{v}_i(t) + C_{2i}(\eta_i, \dot{\eta}_i)v_i(t) + D_{2i}(\eta_i)v_i(t) + \tau_{d2i}(t) = B_{2i}(\eta_i)\tau_{ai}, \quad (3)$$

where $M_{2i}(\eta_i) = S_i^T(\eta_i)M_{1i}(\eta_i)S_i(\eta_i)$,, $C_{2i}(\eta_i, \dot{\eta}_i) = S_i^T(\eta_i)M_{1i}(\eta_i)\dot{S}_i(\eta_i) + S_i^T(\eta_i)C_{1i}(\eta_i, \dot{\eta}_i)S_i(\eta_i)$, $D_{2i}(\eta_i) = S_i^T(\eta_i)D_{1i}S_i(\eta_i)$, $\tau_{d2i}(t) = S_i^T(\eta_i)\tau_{d1i}(t)$ and $B_{2i}(\eta_i) = S_i^T(\eta_i)B_{1i}(\eta_i)$.

2.3. Leader–follower formation

The main objective of the virtual leader–follower formation control strategy, which is discussed in this paper, is to design a high-performance PID formation tracking controller under following requirements: (i) each follower i tracks the virtual leader such that $\lim_{t\to\infty}|\rho_i(t) - \rho_{id}(t)| \le \varepsilon_\rho$ and $\lim_{t\to\infty}|\varphi_i(t) - \varphi_{id}(t)| \le \varepsilon_\varphi$ where ρ_i and φ_i are the virtual range (separation) and bearing angle of ith follower with respect to the virtual leader whose motion equations are specified by $\dot{\eta}_d = S_d(\eta_d)v_d$ and $M_2(\eta_d)\dot{v}_d + C_2(\eta_d, \dot{\eta}_d)v_d + D_2v_d = B_2(\eta_d)\tau_{ad}$ where η_d, v_d, and τ_{ad} denote desired posture, velocity, and torque for the virtual leader, respectively. In addition, ρ_{id} and φ_{id} show the desired virtual range and bearing angle, respectively, and ε_ρ and ε_φ are arbitrary small positive constants; (ii) the robustness of the formation controller is guaranteed against uncertain dynamics, modeling errors, and environmental disturbances; (iii) velocity measurements of followers are not required in real time. To obtain these control objectives, following assumptions are essential:

Assumption 1: The postures of all CLMRs, i.e. $\eta_i \in \mathfrak{R}^4$, are measurable in real-time and velocity signals are not available for the feedback.

Assumption 2: The desired formation vector $q_{id}(t) = [\rho_{id}(t), \phi_{id}(t)]^T$, and its derivatives $\dot{q}_{id}(t)$ and $\ddot{q}_{id}(t)$ are bounded signals such that $\sup_{t\ge0}\|q_{id}(t)\| < B_{dp}$, $\sup_{t\ge0}\|\dot{q}_{id}(t)\| < B_{dv}$ and $\sup_{t\ge0}\|\ddot{q}_{id}(t)\| < B_{da}$ where B_{dp}, B_{dv}, and B_{da} are unknown positive constants.

Assumption 3: The desired torque signal, i.e. $\tau_{ad}(t)$, is bounded such that $\sup_{t\ge0}\|\tau_{ad}(t)\| < B_{d\tau}$ where $B_{d\tau}$ is a positive scalar.

Assumption 4: The external time-varying disturbance, i.e. $\tau_{d1i}(t)$, is also bounded.

Remark 1: According to Assumption 1, position and orientation sensors are available in practice to measure real-time posture of all robots. However, velocity sensors are often excluded to save the weight and the cost of robots which, in turn, it shows the necessity of an OFB controller in this paper. Assumption 2 is used to prove the boundedness of closed-loop signals in the next section. In fact, this assumption is given to support the convergence of the formation configuration. In scenarios that the user chooses unbounded signals such as $q_{id}(t) = [at, bt]^T$, $\forall a, b \in \mathfrak{R}$, the formation diverges gradually in time in spite of the controller stability. Assumption 3 is provided to guarantee that the posture, velocity, and acceleration of the virtual leader are bounded signals. In the next section, this assumption is also employed to prove the boundedness of closed-loop signals. In this case, if the user chooses unbounded signals for $\tau_{ad}(t)$ (such as ramp signal), the control system may lose its stability. Assumption 4 expresses the boundedness of the external disturbance. Since external disturbances in real-world experiments often emerge from friction, unmodeled dynamics, bounded environmental torques and forces, the validity of Assumption 4 is also justified in practice. This assumption is necessary for the design of adaptive robust controller in the next section. Otherwise, in the presence of unbounded disturbances (e.g. $\tau_{di}(t) = \beta e^{\alpha t}$ with $\alpha > 0$), the controller may lose its stability.

To solve the leader–follower formation control problem in the next section, a new second-order leader–follower formation model is introduced here which inherits all structural properties of CLMRs dynamics. According to Figure 1, posture errors between ith follower and the virtual leader in the earth-fixed frame $\{O_E, X_E, Y_E\}$ are

transformed to the body-fixed frame $\{O_{Bi}, X_{Bi}, Y_{Bi}\}$ by the following transformation:

$$e_i(t) = \begin{bmatrix} e_{i1}(t) \\ e_{i2}(t) \\ e_{i3}(t) \\ e_{i4}(t) \end{bmatrix} = \underbrace{\begin{bmatrix} \cos\psi_i & \sin\psi_i & 0 & 0 \\ -\sin\psi_i & \cos\psi_i & 0 & 0 \\ 0 & 0 & 1 & 0 \\ 0 & 0 & 0 & 1 \end{bmatrix}}_{T_i(\psi_i)} \underbrace{\begin{bmatrix} x_d(t) - x_i(t) \\ y_d(t) - y_i(t) \\ \psi_d(t) - \psi_i(t) \\ \gamma_d(t) - \gamma_i(t) \end{bmatrix}}_{\eta_d(t) - \eta_i(t)}. \tag{4}$$

Differentiating (4) yields the following error dynamics in the body-fixed frame:

$$\begin{bmatrix} \dot{e}_{i1}(t) \\ \dot{e}_{i2}(t) \\ \dot{e}_{i3}(t) \\ \dot{e}_{i4}(t) \end{bmatrix} = \begin{bmatrix} -v_i + v_d \cos e_{i3} + (v_i e_{i2}/a_i)\tan\gamma_i \\ -(v_i e_{i1}/a_i)\tan\gamma_i + v_d \sin e_{i3} \\ (v_d/a_d)\tan\gamma_d - (v_i/a_i)\tan\gamma_i \\ \omega_d - \omega_i \end{bmatrix}. \tag{5}$$

Now, we re-write (5) as follows:

$$\begin{bmatrix} \dot{e}_{i1}(t) \\ \dot{e}_{i2}(t) \\ \dot{e}_{i3}(t) \\ \dot{e}_{i4}(t) \end{bmatrix} = \underbrace{\begin{bmatrix} -1 + (e_{i2}/a_i)\tan(\gamma_d - e_{i4}) & 0 \\ -(e_{i1}/a_i)\tan(\gamma_d - e_{i4}) & 0 \\ -(1/a_i)\tan(\gamma_d - e_{i4}) & 0 \\ 0 & -1 \end{bmatrix}}_{J_i(e_i,\gamma_d)} \underbrace{\begin{bmatrix} v_i \\ \omega_i \end{bmatrix}}_{v_i} + \underbrace{\begin{bmatrix} \cos e_{i3} & 0 \\ \sin e_{i3} & 0 \\ 1/a_d \tan\gamma_d & 0 \\ 0 & 1 \end{bmatrix}}_{S_i(e_{i3},\gamma_d)} \underbrace{\begin{bmatrix} v_d \\ \omega_d \end{bmatrix}}_{v_d}. \tag{6}$$

Then, the virtual range and bearing angle of the middle point of ith CLMR front wheels with respect to the virtual leader are defined as follows:

$$q_i(t) = h(e_i) = \begin{bmatrix} \rho_i(t) \\ \varphi_i(t) \end{bmatrix} = \begin{bmatrix} \rho_i(t) \\ \phi_i(t) - \gamma_i(t) \end{bmatrix} = \begin{bmatrix} \sqrt{(e_{i1}(t) - a_i)^2 + e_{i2}^2(t)} \\ atan2(e_{i2}(t), e_{i1}(t) - a_i) - \gamma_i(t) \end{bmatrix}, \tag{7}$$

where $atan2(y, x)$ returns the arc tangent of y/x within $(-\pi, \pi]$. By differentiating (7) and replacing (6), one gets

$$\dot{q}_i(t) = \underbrace{\begin{bmatrix} -\cos\phi_i - \sin\phi_i \tan(\gamma_d - e_{i4}) & 0 \\ (\sin\phi_i - \cos\phi_i \tan(\gamma_d - e_{i4}))/\rho_i - \tan(\gamma_d - e_{i4})/a_i & -1 \end{bmatrix}}_{R_i(e_i,\gamma_d)} v_i + \underbrace{\begin{bmatrix} v_d \cos(e_{i3} - \phi_i) \\ v_d \sin(e_{i3} - \phi_i)/\rho_i \end{bmatrix}}_{\delta_i(e_i,v_d)}. \tag{8}$$

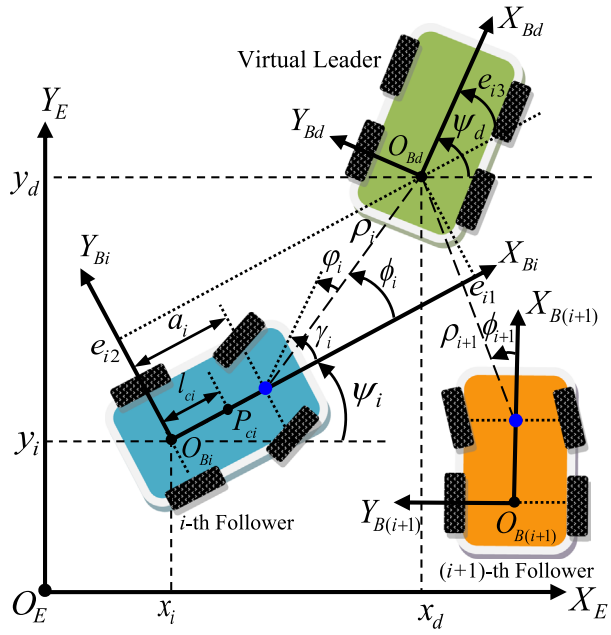

Figure 1. The planar formation configuration of N CLMRs.

The time derivative of (8) yields $\ddot{q}_i = \dot{R}_i v_i + R_i \dot{v}_i + \dot{\delta}_i$ that is expressed as $\dot{v}_i = R_i^{-1}\ddot{q}_i - R_i^{-1}\dot{R}_i v_i - R_i^{-1}\delta_i$ which together with $v_i = R_i^{-1}\dot{q}_i - R_i^{-1}\delta_i$ from (8), and (3) yield

$$\begin{aligned} &M_{2i}R_i^{-1}\ddot{q}_i - M_{2i}R_i^{-1}\dot{R}_i(R_i^{-1}\dot{q}_i - R_i^{-1}\delta_i) \\ &- M_{2i}R_i^{-1}\dot{\delta}_i + C_{2i}R_i^{-1}\dot{q}_i - C_{2i}R_i^{-1}\delta_i \\ &+ D_{2i}R_i^{-1}\dot{q}_i - D_{2i}R_i^{-1}\delta_i + \tau_{d2i} = B_{2i}\tau_{ai}. \end{aligned} \tag{9}$$

By multiplying both sides of the above equation by R_i^{-T}, and considering $M_{2i}R_i^{-1}\dot{R}_i R_i^{-1}\delta_i - M_{2i}R_i^{-1}\dot{\delta}_i = -M_{2i}d(R_i^{-1}\delta_i)/\mathrm{d}t$ and

$$\begin{aligned} d(R_i^{-1}\delta_i)/\mathrm{d}t &= \partial(R_i^{-1}\delta_i)/\partial e_i J_i(e_i,\gamma_d)R_i^{-1}\dot{q}_i \\ &- \partial(R_i^{-1}\delta_i)/\partial e_i J_i(e_i,\gamma_d)R_i^{-1}\delta_i \\ &+ \partial(R_i^{-1}\delta_i)/\partial e_i S_i(e_{i3},\gamma_d)v_d \\ &+ \partial(R_i^{-1}\delta_i)/\partial v_d\dot{v}_d + \partial(R_i^{-1}\delta_i)/\partial\gamma_d\dot{\gamma}_d, \end{aligned}$$

the following second-order leader–follower formation model is derived:

$$\begin{aligned} &M_i(e_i,\gamma_d)\ddot{q}_i + C_i(e_i,\gamma_d,\dot{q}_i)\dot{q}_i + D_i(e_i,\gamma_d)\dot{q}_i \\ &- \bar{D}_i(e_i,\gamma_d,v_d)\dot{q}_i + f_i + \tau_{di}(t) = B_i(e_i,\gamma_d)\tau_{ai} = \bar{\tau}_{ai}, \end{aligned} \tag{10}$$

where $M_i(e_i,\gamma_d) = R_i^{-T}(e_i,\gamma_d)M_{2i}R_i^{-1}(e_i,\gamma_d)$, $C_i(e_i,\gamma_d,\dot{q}_i) = R_i^{-T}(C_{2i}(R_i^{-1}\dot{q}_i) - M_{2i}R_i^{-1}\dot{R}_i)R_i^{-1}$, $D_i(e_i,\gamma_d) = R_i^{-T}(e_i,\gamma_d)D_{2i}R_i^{-1}(e_i,\gamma_d)$, $\tau_{di}(t) = R_i^{-T}(e_i,\gamma_d)\tau_{d2i}(t)$, $B_i(e_i,\gamma_d) = R_i^{-T}(e_i,\gamma_d)B_{2i}$ and

$$\bar{D}_i(e_i,\gamma_d,\upsilon_d) = R_i^{-T}(M_{2i}\partial(R_i^{-1}\delta_i)/\partial e_i J_i(e_i,\gamma_d) + 2C_{2i}(R_i^{-1}\delta_i))R_i^{-1},$$

$$\begin{aligned} f_i(e_i,\gamma_d,\nu_d,\dot{\nu}_d) = {} & R_i^{-T}M_{2i}\partial(R_i^{-1}\delta_i)/\partial e_i J_i(e_i,\gamma_d)R_i^{-1}\delta_i \\ & - R_i^{-T}M_{2i}\partial(R_i^{-1}\delta_i)/\partial e_i S_i(e_{i3},\gamma_d)\nu_d \\ & - R_i^{-T}M_{2i}\partial(R_i^{-1}\delta_i)/\partial \upsilon_d\dot{\upsilon}_d \\ & - R_i^{-T}M_{2i}\partial(R_i^{-1}\delta_i)/\partial\gamma_d\dot{\gamma}_d \\ & + R_i^{-T}C_{2i}(R_i^{-1}\delta_i)R_i^{-1}\delta_i - R_i^{-T}D_{2i}R_i^{-1}\delta_i. \end{aligned}$$

Provided that R_i is invertible, and recalling structural properties of model (3) from [22,25], following properties can be easily proven for model (10):

Property 1: The matrix $M_i(e_i, \gamma_d)$ is symmetric and positive-definite such that $\lambda_{mi}\|x\|^2 \le x^T M_i x \le \lambda_{Mi}\|x\|^2$, $\forall x \in \mathfrak{R}^2$, $e_i \in \mathfrak{R}^4$, $\gamma_d \in \mathfrak{R}$ where $0 < \lambda_{mi} \le \lambda_{Mi} < \infty$, $\lambda_{mi} := \min_{\forall e_i\in\mathfrak{R}^4,\gamma_d\in\mathfrak{R}}\lambda_{\min}(M_i(e_i,\gamma_d))$, and $\lambda_{Mi} := \max_{\forall e_i\in\mathfrak{R}^4,\gamma_d\in\mathfrak{R}}\lambda_{\max}(M_i(e_i,\gamma_d))$.

Property 2: The Coriolis matrix satisfies the following $\forall x_1, x_2, y, \dot{q}_i \in \mathfrak{R}^2$, $e_i \in \mathfrak{R}^4$, $\gamma_d \in \mathfrak{R}$:

(2.1) $x_1^T(\dot{M}_i(e_i,\gamma_d) - 2C_i(e_i,\gamma_d,\dot{q}_i))x_1 = 0$;
(2.2) $C_i(e_i,\gamma_d,x_1)x_2 = C_i(e_i,\gamma_d,x_2)x_1$;
(2.3) $C_i(e_i,\gamma_d,x_1+x_2)y = C_i(e_i,\gamma_d,x_1)y + C_i(e_i,\gamma_d,x_2)y$;
(2.4) $\|C_i(e_i,\gamma_d,x_1)x_2\| \le \lambda_{Ci}\|x_1\|\|x_2\|, \forall\lambda_{Ci} \ge 0$.

Property 3: The damping matrix $D_i(e_i, \gamma_d)$ is symmetric and positive-definite such that $\lambda_{di}\|x\|^2 \le x^T D_i x \le \lambda_{Di}\|x\|^2, \forall x\in\mathfrak{R}^2, e_i\in\mathfrak{R}^4, \gamma_d\in\mathfrak{R}$ where $0 < \lambda_{di} \le \lambda_{Di} < \infty$, $\lambda_{di} := \min_{\forall e_i\in\mathfrak{R}^4,\gamma_d\in\mathfrak{R}}\lambda_{\min}(D_i(e_i,\gamma_d))$, and $\lambda_{Di} := \max_{\forall e_i\in\mathfrak{R}^4,\gamma_d\in\mathfrak{R}}\lambda_{\max}(D_i(e_i,\gamma_d))$.

Property 4: The external disturbance term is bounded as $\|\tau_{di}(t)\| \le \lambda_{\tau di}$ where $\lambda_{\tau di}$ is a positive unknown constant.

2.4. RBFNN approximator

In this section, RBFNN is introduced to approximate uncertain nonlinearities of nonholonomic CLMRs in the next section. From a review of [23,26] and references therein, this technique is widely used to estimate unknown nonlinear functions. Figure 2 shows the structure of a three-layer RBFNN. Consider an arbitrary continuous function $f(x)$: $\mathfrak{R}^{n_i} \to \mathfrak{R}^p$. Then, there exists an RBF neural network such that

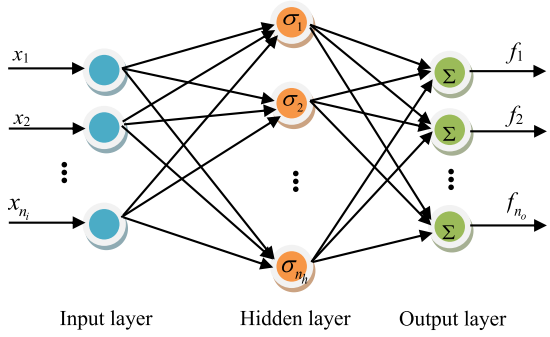

Figure 2. The structure of radial basis function neural network.

$$\begin{cases} f_m(x) = \sum_{k=1}^{n_h} w_{mk}\sigma_k(x) + e_{wm}, \quad m = 1,2,\ldots,n_o, \quad \forall x \in \mathfrak{R}^{n_i}, \\ \sigma_k(x) = \exp\left(-(x-\mu_k)^T(x-\mu_k)/\lambda_k^2\right), \quad k = 1,2,\ldots,n_h, \end{cases} \tag{11}$$

that can be written in the matrix form $f(x) = W\sigma(x) + e_w(x)$ where $f(x) = \left[f_1(x),\ldots,f_{n_o}(x)\right]^T$, $x \in \mathfrak{R}^{n_i}$ shows the input vector, $W \in \mathfrak{R}^{n_o\times n_h}$ represents NN weights matrix, n_h and n_o denote the number of hidden nodes and output nodes, respectively, $\sigma(x) = \left[\sigma_1(x),\ldots,\sigma_{n_h}(x)\right]^T$, where $\sigma_k(x)$ is kth Gaussian basis function, $\mu_k = \left[\mu_{k1},\mu_{k2},\ldots,\mu_{kn_i}\right]^T$ and λ_k show the center vector and standard deviation, respectively, and $e_w = \left[e_{w1},e_{w2},\ldots,e_{wn_o}\right]^T$ represents the approximation error vector which is bounded over a compact set $U \subset \mathfrak{R}^{n_i}$ such that $\|e_w\| \le B_w$, $\forall x \in U \subset \mathfrak{R}^{n_i}$ where B_w denotes an unknown positive constant. Based on the universal approximation property of RBFNNs [26], there exists an ideal NN weight matrix W^* which minimizes $\|e_w\|$ for all $x \in U \subset \mathfrak{R}^{n_i}$ such that

$$\begin{cases} f(x) = W^*\sigma(x) + e_w^*(x), \quad \forall x \in U \subset \mathfrak{R}^{n_i}, \\ W^* := \arg\min_{W\in\mathfrak{R}^{n_o\times n_h}}\left\{\sup_{x\in U}\|f(x) - W\sigma(x)\|\right\}, \end{cases} \tag{12}$$

where $e_w^*(x)$ is the approximation error for $W = W^*$. However, the ideal NN weight matrix W^* is unknown in general. Thus, a learning mechanism is often used to approximate NN weights matrix, i.e. $\hat{W}$. This helps the user estimate the unknown nonlinear function as $\hat{f}(x) = \hat{W}\sigma(x)$ where $\hat{W}$ is usually updated by a suitable adaptive law. The following assumption is necessary in the design of RBFNN-based approximators:

Assumption 5: The ideal NN weights are bounded on the compact set $U \subset \mathfrak{R}^{n_i}$ in the sense that $\|W^*\|_F \le W_M$, where W_M represents an unknown positive constant.

3. Main results

3.1. Neural adaptive OFB-PID formation controller design

In this section, a formation controller is proposed to obtain all control objectives of Section 2.3. To design a high performance formation control system, a new PID velocity observer-based control strategy and projection-type neural adaptive robust techniques are introduced here. To start our design, the tracking error is defined as $\varepsilon_i(t) := q_i(t) - q_{id}(t)$ and the observation error is denoted by $\tilde{q}_i(t) := q_i(t) - \hat{q}_i(t)$. Then, the following filtered tracking error variables are introduced:

$$s_{ic}(t) := \dot{\xi}_{ic}(t) + \beta_i \xi_{ic}(t), \tag{13}$$

$$\xi_{ic}(t) := \varepsilon_i(t) + \alpha_i \int_0^t \varepsilon_i(\tau)\mathrm{d}\tau. \tag{14}$$

For the purpose of the observer design, filtered observation error variables are also defined as follows:

$$s_{io}(t) := \dot{\xi}_{io}(t) + \beta_i \xi_{io}(t), \tag{15}$$

$$\xi_{io}(t) := \tilde{q}_i(t) + \alpha_i \int_0^t \tilde{q}_i(\tau)\mathrm{d}\tau. \tag{16}$$

The tracking and observation error variables (13)–(16) are equivalent to the following filtered error variables:

$$s_{ic}(t) := \dot{\varepsilon}_i(t) + \Lambda_{i0}\varepsilon_i(t) + \Lambda_{i1}\int_0^t \varepsilon_i(\tau)\mathrm{d}\tau, \tag{17}$$

$$s_{io}(t) := \dot{\tilde{q}}_i(t) + \Lambda_{i0}\tilde{q}_i(t) + \Lambda_{i1}\int_0^t \tilde{q}_i(\tau)\mathrm{d}\tau, \tag{18}$$

where $\Lambda_{i0} = (\alpha_i + \beta_i)I_2$ and $\Lambda_{i1} = \alpha_i\beta_i I_2$ are positive-definite gain matrices and $\alpha_i, \beta_i \in \mathfrak{R}^+$. By substituting (17) into (10) and applying Properties 2.3 and 2.4, one obtains

$$\begin{aligned} M_i(e_i,\gamma_d)\dot{s}_{ic} = {} & -C_i(e_i,\gamma_d,\dot{q}_i)s_{ic} - D_i(e_i,\gamma_d)s_{ic} \\ & + B_i(e_i,\gamma_d)\tau_{ai} + \eta_i - \tau_{di}(t) + \chi_{1i}, \end{aligned} \tag{19}$$

where η_i is given by

$$\begin{aligned} \eta_i = {} & -M_i(e_i,\gamma_d)\ddot{q}_{id} - C_i(e_i,\gamma_d,\dot{q}_{id})\dot{q}_{id} - D_i(e_i,\gamma_d)\dot{q}_{id} \\ & + \bar{D}_i(e_i,\gamma_d,\upsilon_d)\dot{q}_{id} - f_i(e_i,\gamma_d,\nu_d,\dot{\nu}_d) \end{aligned} \tag{20}$$

and χ_{1i} is defined as follows:

$$\begin{aligned} \chi_{1i} = {} & M_i(e_i,\gamma_d)\Lambda_{i0}\dot{\varepsilon}_i + M_i(e_i,\gamma_d)\Lambda_{i1}\varepsilon_i + C_i(e_i,\gamma_d,\dot{q}_i)\Lambda_{i0}\varepsilon_i \\ & - C_i(e_i,\gamma_d,\dot{q}_{id})\dot{\varepsilon}_i + C_i(e_i,\gamma_d,\dot{q}_i)\Lambda_{i1}\int_0^t \varepsilon_i(\tau)\mathrm{d}\tau \\ & + D_i(e_i,\gamma_d)\Lambda_{i0}\varepsilon_i + D_i(e_i,\gamma_d)\Lambda_{i1}\int_0^t \varepsilon_i(\tau)\mathrm{d}\tau \\ & + \bar{D}_i(e_i,\gamma_d,\upsilon_d)s_{ic} - \bar{D}_i(e_i,\gamma_d,\upsilon_d)\Lambda_{i0}\varepsilon_i \\ & - \bar{D}_i(e_i,\gamma_d,\upsilon_d)\Lambda_{i1}\int_0^t \varepsilon_i(\tau)\mathrm{d}\tau,. \end{aligned} \tag{21}$$

One may write the following upper bound for $\chi_{1i} \in \mathfrak{R}^n$ using Properties 1, 2.4 and 3

$$\|\chi_{1i}\| \le c_{1i}\|x_i\| + c_{2i}\|x_i\|^2, \tag{22}$$

where c_{1i} and c_{2i} are positive constants and $x_i \in \mathfrak{R}^{12}$ is defined as follows:

$$x_i(t) := \left[\xi_{ic}^T(t), \xi_{io}^T(t), \varepsilon_i^T(t), \tilde{q}_i^T(t), s_{ic}^T(t), s_{io}^T(t)\right]^T. \tag{23}$$

By defining $x_{wi} = [e_i^T, \gamma_d, \nu_d^T, \dot{\nu}_d^T, \dot{q}_{id}^T, \ddot{q}_{id}^T]^T$ and using the approximation property of RBFNNs, the unknown function $\eta_i(x_{wi})$ is approximated as $\eta_i(x_{wi}) = W_i^*\sigma(x_{wi}) + e_{wi}$ where $\|e_{wi}\| \le B_{wi}$. Then, the following neural OFB-PID formation controller is proposed:

$$\tau_{ai} = B_{2i}^{-1}R_i^T\left(\underbrace{-K_{ip}\dot{\hat{\varepsilon}}_i(t) - K_{ip}\Lambda_{i0}\hat{\varepsilon}_i(t) - K_{ip}\Lambda_{i1}\int_0^t \hat{\varepsilon}_i(\tau)\mathrm{d}\tau}_{-K_{ip}\left(s_{ic}(t) - s_{io}(t)\right)} - \hat{W}_i\sigma(x_{wi}) - \frac{(\hat{s}_{ic} + \hat{s}_{io})\hat{\theta}_i^2}{\hat{\theta}_i\|\hat{s}_{ic} + \hat{s}_{io}\| + \varepsilon_{ti}}\right), \tag{24}$$

where PID terms are derived by subtracting (17) from (18), $\hat{\varepsilon}_i := \hat{q}_i - q_{id} \in \mathfrak{R}^2$ and $\dot{\hat{\varepsilon}}_i := R_i\hat{v}_i + \delta_i - \dot{q}_{id}$ denote the estimated tracking error vector and its derivative, respectively, $K_{ip} \in \mathfrak{R}^{2\times 2}$ is a positive-definite diagonal gain matrix, $\hat{\theta}_i \in \mathfrak{R}$ is the estimation of θ_i which is defined later, the signal $(\hat{s}_{ic} + \hat{s}_{io}) \in \mathfrak{R}^2$ represents the approximation of $s_{ic} + s_{io}$ which is defined as follows:

$$\hat{s}_{ic} + \hat{s}_{io} := \dot{\hat{\varepsilon}}_i + \Lambda_{i0}\left(\varepsilon_i + \tilde{q}_i\right) + \Lambda_{i1}\int_0^t \left(\varepsilon_i(\tau) + \tilde{q}_i(\tau)\right)\mathrm{d}\tau, \tag{25}$$

and the approximation error is given by

$$\tilde{s}_{ic} + \tilde{s}_{io} := s_{ic} + s_{io} - (\hat{s}_{ic} + \hat{s}_{io}) = 2\left(s_{io} - \Lambda_{i0}\tilde{q}_i - \Lambda_{i1}\int_0^t \tilde{q}_i(\tau)\mathrm{d}\tau\right). \tag{26}$$

The term $\tilde{s}_{ic} + \tilde{s}_{io}$ is bounded as follows:

$$\|\tilde{s}_{ic} + \tilde{s}_{io}\| \leq c_{3i}\|x_i\|, \tag{27}$$

where $c_{3i} \in \Re^+$. In the proposed controller (24), $\hat{W}_i \in \Re^{n_o \times n_h}$ ($n_o = 2$) and $\hat{\theta}_i \in \Re$ are updated by

$$\dot{\hat{W}}_i = \text{Proj}_{\hat{W}_i}\left(\gamma_{wi}(\hat{s}_{ic} + \hat{s}_{io})\sigma^T(x_{wi})\right), \quad \dot{\hat{\theta}}_i = \text{Proj}_{\hat{\theta}_i}\left(\gamma_{\theta i}\|\hat{s}_{ic} + \hat{s}_{io}\|\right) \tag{28}$$

which are defined as follows:

$$\text{Proj}_{\hat{W}_i}\left(\gamma_{wi}(\hat{s}_{ic} + \hat{s}_{io})\sigma^T(x_{wi})\right) = \begin{cases} \gamma_{wi}(\hat{s}_{ic} + \hat{s}_{io})\sigma^T, \text{ if } \text{tr}\{\hat{W}_i^T\hat{W}_i\} < W_{mi} \\ \text{or if } \text{tr}\{\hat{W}_i^T\hat{W}_i\} = W_{mi} \text{ and } \sigma^T\hat{W}_i^T(\hat{s}_{ic} + \hat{s}_{io}) \leq 0; \\ \gamma_{wi}(\hat{s}_{ic} + \hat{s}_{io})\sigma^T - \gamma_{wi}\frac{\sigma^T\hat{W}_i^T(\hat{s}_{ic}+\hat{s}_{io})}{\text{tr}\{\hat{W}_i^T\hat{W}_i\}}\hat{W}_i, \\ \text{if } \text{tr}\{\hat{W}_i^T\hat{W}_i\} = W_{mi} \text{ and } \sigma^T\hat{W}_i^T(\hat{s}_{ic} + \hat{s}_{io}) > 0; \end{cases} \tag{29}$$

$$\text{Proj}_{\hat{\theta}_i}\left(\gamma_{\theta i}\|\hat{s}_{ic} + \hat{s}_{io}\|\right) = \begin{cases} \gamma_{\theta i}\|\hat{s}_{ic} + \hat{s}_{io}\|, & \text{if } \hat{\theta}_i < \theta_{mi} \\ 0, & \text{if } \hat{\theta}_i = \theta_{mi} \end{cases}, \tag{30}$$

where $\hat{\theta}_i(0) \in \Omega_{\theta i} = \{\hat{\theta}_i \in \Re : 0 \leq \hat{\theta}_i \leq \theta_{mi}\}$, and $\gamma_{wi}, \gamma_{\theta i} \in \Re^+$ denote adaptation gains. Then, the closed-loop error dynamics is obtained as follows by substituting (24) into (19):

$$\begin{aligned} M_i(e_i, \gamma_d)\dot{s}_{ic} = &-C_i(e_i, \gamma_d, \dot{q}_i)s_{ic} - D_i(e_i, \gamma_d)s_{ic} \\ &- K_{ip}(s_{ic} - s_{io}) - (\hat{s}_{ic} + \hat{s}_{io})\hat{\theta}_i^2/ \\ &(\hat{\theta}_i\|\hat{s}_{ic} + \hat{s}_{io}\| + \varepsilon_{ti}) + \tilde{W}_i\sigma(x_{wi}) + e_{wi} \\ &- \tau_{di}(t) + \chi_{1i}, \end{aligned} \tag{31}$$

where $\tilde{W}_i := W_i^* - \hat{W}_i$ denotes the weights estimation error matrix and $e_{wi} - \tau_{di}(t)$ is bounded as $\|e_{wi} - \tau_{di}(t)\| \leq \theta$. Motivated by [21], the following velocity observer is proposed in this paper:

$$\hat{v}_i(t) = R_i^{-1}(e_i, \gamma_d)(p_i(t) + \Lambda_{i0}\tilde{q}_i(t) + k_{id}\tilde{q}_i(t) - \delta_i(e_i, v_d)), \tag{32}$$

$$\dot{p}_i(t) = \ddot{q}_{id}(t) + k_{id}\Lambda_{i0}\tilde{q}_i(t) + \Lambda_{i1}\tilde{q}_i(t) + \zeta_i(t), \quad p_i(0) = p_{i0}, \tag{33}$$

$$\dot{\zeta}_i(t) = k_{id}\Lambda_{i1}\tilde{q}_i(t), \quad \zeta_i(0) = \zeta_{i0}, \tag{34}$$

where $k_{id} \in \Re^+$ is the observer gain which is a positive real constant. Initial conditions of the observer are chosen as $p_{i0} = p_i(0) = -\Lambda_{i0}\tilde{q}_i(0) - k_{id}\tilde{q}_i(0)$, and $\hat{q}_i(0) = q_i(0)$ to have $\tilde{q}_i(0) = 0$, and $\dot{\hat{q}}_i(0) = 0$. Since from (8) and (32), one may write $\ddot{\tilde{q}}_i(t) = \dot{p}_i(t) + \Lambda_{i0}\dot{\tilde{q}}_i(t) + k_{id}\dot{\tilde{q}}_i(t)$, it is easy to show that (32)–(34) are equivalent to

$$\dot{s}_{ic}(t) = \dot{s}_{io}(t) + k_{id}s_{io}(t) + \Lambda_{i0}\dot{e}_i(t) + \Lambda_{i1}e_i(t). \tag{35}$$

By substituting (35) into (31) and recalling Properties 2.2 and 2.3, the following observer error equation is obtained:

$$\begin{aligned} M_i(e_i, \gamma_d)\dot{s}_{io} = &-C_i(e_i, \gamma_d, \dot{q}_i)s_{io} - k_{id}M_i(e_i, \gamma_d)s_{io} \\ &- K_{ip}(s_{ic} - s_{io}) - (\hat{s}_{ic} + \hat{s}_{io})\hat{\theta}_i^2/ \\ &(\hat{\theta}_i\|\hat{s}_{ic} + \hat{s}_{io}\| + \varepsilon_{ti}) + \tilde{W}_i\sigma(x_{wi}) + e_{wi} \\ &- \tau_{di}(t) + \chi_{2i}, \end{aligned} \tag{36}$$

where χ_{2i} is given by

$$\begin{aligned} \chi_{2i} = &C_i(e_i, \gamma_d, \dot{q}_i)s_{io} - D_i(e_i, \gamma_d)s_{ic} - C_i(e_i, \gamma_d, \dot{q}_i)s_{ic} \\ &+ C_i(e_i, \gamma_d, \dot{q}_i)\Lambda_{i0}\varepsilon_i - C_i(e_i, \gamma_d, \dot{q}_{id})\dot{\varepsilon}_i \\ &+ C_i(e_i, \gamma_d, \dot{q}_i)\Lambda_{i1}\int_0^t \varepsilon_i(\tau)\text{d}\tau \\ &+ D_i(e_i, \gamma_d)\Lambda_{i0}\varepsilon_i + D_i(e_i, \gamma_d)\Lambda_{i1}\int_0^t \varepsilon_i(\tau)\text{d}\tau \\ &+ \bar{D}_i(e_i, \gamma_d, v_d)s_{ic} - \bar{D}_i(e_i, \gamma_d, v_d)\Lambda_{i0}\varepsilon_i \\ &- \bar{D}_i(e_i, \gamma_d, v_d)\Lambda_{i1}\int_0^t \varepsilon_i(\tau)\text{d}\tau. \end{aligned} \tag{37}$$

From (14), (16), (17), (18), and (23) and Properties 2.4 and 3, the following upper bound is achieved for χ_{2i}:

$$\|\chi_{2i}\| \leq c_{4i}\|x_i\| + c_{5i}\|x_i\|^2, \tag{38}$$

where c_{4i} and c_{5i} are positive constants. It should be noted that the bounds in (22), (27), and (38) are only useful for the stability analysis and they are not required for the implementation of the proposed controller. Figure 3 demonstrates a block diagram of the proposed control scheme.

3.2. Stability analysis

Based on presented developments in the previous section, the stability of the closed-loop OFB-PID formation control system is summarized by the following theorem:

Theorem 1: *Consider the kinematic and dynamic models of a team of N CLMRs which are denoted by (2) and (3).*

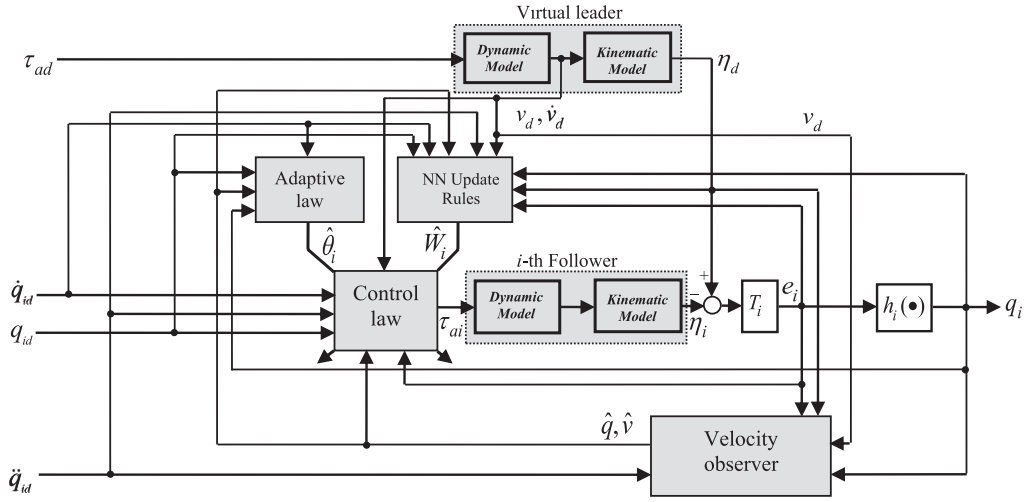

Figure 3. A block diagram of the proposed output-feedback formation control system.

Given a bounded continuous desired trajectory which is generated by a virtual robot and given a desired formation configuration, under Assumptions 1–5 and the formation model (10), if gains of the OFB-PID formation controller (24), (25), (28)–(30), and (32)–(34) are chosen to satisfy following conditions

$$\alpha_i\lambda_{\min}(K_{ip}) > 0.5\lambda_{\max}(K_{ip})/\ell + 0.5\beta_i\lambda_{\max}(K_{ip})/\ell, \quad (39)$$

$$\beta_i\lambda_{\min}(K_{ip}) > 0.5\lambda_{\max}(K_{ip})/\ell + 0.5\beta_i\ell\,\lambda_{\max}(K_{ip}), \quad (40)$$

$$\lambda_{\min}(K_{ip} + D_i) > \ell\,\lambda_{\max}(K_{ip}) + 0.5\ell\left(c_{1i} + c_{2i}\right), \quad (41)$$

$$\lambda_{\min}\left(k_{id}M_i(e_i) - K_{ip}\right) > \ell\,\lambda_{\max}(K_{ip}) + 0.5\ell\left(c_{4i} + c_{5i}\right), \quad (42)$$

$\forall \ell \in \mathfrak{R}^+$*, then, the proposed neural adaptive OFB-PID formation controller guaranties that all signals in the resulting closed-loop system are bounded and the tracking and state observation errors are SGUUB. Moreover, the region of attraction*

$$R_A = \left\{ \vartheta(t) \in \mathfrak{R}^P \,\middle|\, \|\vartheta(t)\| < \sqrt{\lambda_{x\min}\left(\kappa_m - \kappa_7\right)/\left(\min\left\{\kappa_{8i}\right\}_{i=1}^{N}\lambda_{\vartheta\max}\right)} \right\}$$

can be made arbitrarily large to include any initial condition by selecting large enough control gains, where $P = 12N + N(n_o n_h + 1)$, $\vartheta = [\vartheta_1^T, \vartheta_2^T, \ldots, \vartheta_N^T]^T$, $\vartheta_i = [x_i^T, \tilde{w}_{i,11}, \ldots, \tilde{w}_{i,n_o n_h}, \tilde{\theta}_i]^T$, $\tilde{\theta}_i := \theta_i - \hat{\theta}_i$ *and* κ_m *is a positive gain-dependent parameter,* $x_i \in \mathfrak{R}^{12}$ *was defined in (23) and* $\kappa_7, \kappa_8, \lambda_{x\min}$ *and* $\lambda_{\vartheta\max}$ *will be defined in the sequel.*

***Proof*:** To analyze the stability of the entire formation system, the Lyapunov function candidate is considered as $V(t) = \sum_{i=1}^{N} V_i(\xi_{ic}, \xi_{io}, \varepsilon_i, \tilde{q}_i, s_{ic}, s_{io}, \tilde{W}_i, \tilde{\theta}_i)$ where V_i is given by

$$V_i = \frac{1}{2}\varepsilon_i^T K_{ip}\varepsilon_i + \frac{1}{2}\xi_{ic}^T K_{ip}\xi_{ic} + \frac{1}{2}s_{ic}^T M_i s_{ic} + \frac{1}{2}\tilde{q}_i^T K_{ip}\tilde{q}_i + \frac{1}{2}\xi_{io}^T K_{ip}\xi_{io} + \frac{1}{2}s_{io}^T M_i s_{io} + \frac{1}{2\gamma_{wi}}\mathrm{tr}\left\{\tilde{W}_i^T\tilde{W}_i\right\} + \frac{1}{2\gamma_{\theta i}}\tilde{\theta}_i^2. \quad (43)$$

One may confirm that (43) is bounded as follows:

$$\lambda_{xi}\|x_i\|^2 \le \lambda_{xi}\|x_i\|^2 + 0.5\gamma_{wi}^{-1}\|\tilde{W}_i\|_F^2 + 0.5\gamma_{\theta i}^{-1}\|\tilde{\theta}_i\|^2 \le V_i(t) \le \lambda_{\vartheta i}\|\vartheta_i\|^2, \quad (44)$$

where $\lambda_{xi} = 0.5\min\left\{\lambda_{\min}(K_{ip}), \lambda_{mi}\right\}$, $\lambda_{\vartheta_i} = 0.5\max\left\{\lambda_{\max}(K_{ip}), \lambda_{Mi}, \gamma_{wi}^{-1}, \gamma_{\theta i}^{-1}\right\}$, λ_{mi} and λ_{Mi} are defined in Property 1 and $\vartheta_i = [x_i^T, \tilde{w}_{i,11}, \ldots, \tilde{w}_{i,n_o n_h}, \tilde{\theta}_i]^T$. From (44), it is obvious that $V_i(t)$ is positive-definite, radially unbounded, and decrescent. It should be noted that the overall Lyapunov function is bounded as follow

$$\lambda_{x\min}\|x\|^2 \le V(t) \le \lambda_{\vartheta\max}\|\vartheta\|^2, \quad (45)$$

where $\lambda_{x\min} = \min\{\lambda_{xi}\}_{i=1}^{N}$, $x = [x_1^T, x_2^T, \ldots, x_N^T]^T$, $\lambda_{\vartheta\max} = \max\{\lambda_{\vartheta i}\}_{i=1}^{N}$ and $\vartheta = [\vartheta_1^T, \vartheta_2^T, \ldots, \vartheta_N^T]^T$. By differentiating (43) along (14), (16), (17), (18), (31), and (36), using Property 2.1, recalling (26) and considering that $\dot{\tilde{W}}_i = -\dot{\hat{W}}_i$ and $\dot{\tilde{\theta}}_i = -\dot{\hat{\theta}}_i$, one gets

$$\begin{aligned}\dot{V}_i(t) = {} & \varepsilon_i^T K_{ip}\dot{\varepsilon}_i + \xi_{ic}^T K_{ip}\dot{\xi}_{ic} + s_{ic}^T M_i \dot{s}_{ic} + \frac{1}{2}s_{ic}^T \dot{M} s_{ic} \\ & + \tilde{q}_i^T K_{ip}\dot{\tilde{q}}_i + \xi_{io}^T K_{ip}\dot{\xi}_{io} + s_{io}^T M \dot{s}_{io} + \frac{1}{2}s_{io}^T \dot{M}_i s_{io} \\ & - \frac{1}{\gamma_{wi}}\mathrm{tr}\left\{\tilde{W}_i^T \dot{\hat{W}}_i\right\} - \frac{1}{\gamma_{\theta i}}\tilde{\theta}_i\dot{\hat{\theta}}_i = -\alpha_i \varepsilon_i^T K_{ip}\varepsilon_i \\ & - \beta_i \xi_{ic}^T K_{ip}\xi_{ic} - s_{ic}^T(K_{ip}+D_i)s_{ic} - \alpha_i \tilde{q}_i^T K_{ip}\tilde{q}_i \\ & - \beta_i \xi_{io}^T K_{ip}\xi_{io} - s_{io}^T\left(k_{id}M_i - K_{ip}\right)s_{io} + \varepsilon_i^T K_{ip}s_{ic} \\ & - \beta_i \varepsilon_i^T K_{ip}\xi_{ic} + \xi_{ic}^T K_{ip}s_{ic} + \tilde{q}_i^T K_{ip}s_{io} - \beta_i \tilde{q}_i^T K_{ip}\xi_{io} \\ & + \xi_{io}^T K_{ip}s_{io} + s_{io}^T \chi_{2i} + s_{ic}^T \chi_{1i} + \delta_i + (\hat{s}_{ic}+\hat{s}_{io})^T \\ & \left(e_{wi} - \tau_{di}(t)\right) - (\hat{s}_{ic}+\hat{s}_{io})^T(\hat{s}_{ic}+\hat{s}_{io})\hat{\theta}_i^2 / \\ & \left(\hat{\theta}_i\left\|\hat{s}_{ic}+\hat{s}_{io}\right\| + \varepsilon_{ti}\right) + (\hat{s}_{ic}+\hat{s}_{io})^T \tilde{W}_i \sigma(x_{wi}) \\ & - \frac{1}{\gamma_{wi}}\mathrm{tr}\left\{\tilde{W}_i^T \dot{\hat{W}}_i\right\} - \frac{1}{\gamma_{\theta i}}\tilde{\theta}_i\dot{\hat{\theta}}_i,\end{aligned} \tag{46}$$

where δ_i is given by

$$\begin{aligned}\delta_i = {} & (\tilde{s}_{ic}+\tilde{s}_{io})^T \tilde{W}_i \sigma(x_{wi}) + (\tilde{s}_{ic}+\tilde{s}_{io})^T\left(e_{wi} - \tau_{di}(t)\right) \\ & - (\tilde{s}_{ic}+\tilde{s}_{io})^T(\hat{s}_{ic}+\hat{s}_{io})\hat{\theta}_i^2 / \left(\hat{\theta}_i\left\|\hat{s}_{ic}+\hat{s}_{io}\right\| + \varepsilon_{ti}\right),\end{aligned} \tag{47}$$

that is bounded as follows by (27), $2ab \le a^2 + b^2$, $\left\|W_i^*\right\|_F \le W_{Mi}$, $\left\|\hat{W}_i\right\|_F^2 < W_{mi}$ and $\hat{\theta}_i < \theta_{mi}$:

$$\begin{aligned}\left\|\delta_i\right\| \le {} & \frac{3}{2}c_{3i}\left\|x_i\right\|^2 + \frac{1}{2}c_{3i}\left(W_{Mi} + \sqrt{W_{mi}}\right)^2 n_h \\ & + \frac{1}{2}c_{3i}\theta_i^2 + \frac{1}{2}c_{3i}\theta_{mi}^2.\end{aligned} \tag{48}$$

Then, (46) is expressed as follows by substituting (28) into (46):

$$\begin{aligned}\dot{V}_i(t) \le {} & -\alpha_i \lambda_{\min}(K_{ip})\left\|\varepsilon_i\right\|^2 - \beta_i \lambda_{\min}(K_{ip})\left\|\xi_{ic}\right\|^2 \\ & - \lambda_{\min}(K_{ip}+D_i)\left\|s_{ic}\right\|^2 - \alpha_i \lambda_{\min}(K_{ip})\left\|\tilde{q}_i\right\|^2 \\ & - \beta\lambda_{\min}(K_{ip})\left\|\xi_{io}\right\|^2 - \lambda_{\min}\left(k_{id}M_i - K_{ip}\right)\left\|s_{io}\right\|^2 \\ & + \left\|\varepsilon_i\right\|\left\|K_{ip}\right\|\left\|s_{ic}\right\| + \beta_i\left\|\varepsilon_i\right\|\left\|K_{ip}\right\|\left\|\xi_{ic}\right\| \\ & + \left\|\xi_{ic}^T\right\|\left\|K_{ip}\right\|\left\|s_{ic}\right\| + \left\|\tilde{q}_i\right\|\left\|K_{ip}\right\|\left\|s_{io}\right\| + \beta_i\left\|\tilde{q}_i\right\|\left\|K_{ip}\right\|\left\|\xi_{io}\right\| \\ & + \left\|\xi_{io}^T\right\|\left\|K_{ip}\right\|\left\|s_{io}\right\| + \left\|s_{ic}^T\right\|\left\|\chi_{1i}\right\| + \left\|s_{io}^T\right\|\left\|\chi_{2i}\right\| \\ & + \left\|\rho_i\right\| + \left\|\hat{s}_{ic}+\hat{s}_{io}\right\|\left\|e_{wi} - \tau_{di}(t)\right\| \\ & - (\hat{s}_{ic}+\hat{s}_{io})^T(\hat{s}_{ic}+\hat{s}_{io})\hat{\theta}_i^2 / \left(\hat{\theta}_i\left\|\hat{s}_{ic}+\hat{s}_{io}\right\| + \varepsilon_{ti}\right) \\ & + (\hat{s}_{ic}+\hat{s}_{io})^T \tilde{W}_i \sigma(x_{wi}) \\ & - \frac{1}{\gamma_{wi}}\mathrm{tr}\left\{\tilde{W}_i^T \mathrm{Proj}_{\hat{W}_i}\left(\gamma_{wi}(\hat{s}_{ic}+\hat{s}_{io})\sigma^T(x_{wi})\right)\right\} \\ & - \frac{1}{\gamma_{\theta i}}\tilde{\theta}_i \mathrm{Proj}_{\hat{\theta}_i}\left(\gamma_{\theta i}\left\|\hat{s}_{ic}+\hat{s}_{io}\right\|\right),\end{aligned} \tag{49}$$

which together with $\left\|e_{wi} - \tau_{di}(t)\right\| \le \theta_i$, $\theta_i = \tilde{\theta}_i + \hat{\theta}_i$, $ab \le 0.5a^2/\ell + 0.5\ell b^2$, $\forall \ell \in \Re^+$ and following inequalities, which are induced from [27,28],

$$\begin{aligned}&\left\|\hat{s}_{ic}+\hat{s}_{io}\right\|\hat{\theta}_i - (\hat{s}_{ic}+\hat{s}_{io})^T(\hat{s}_{ic}+\hat{s}_{io})\hat{\theta}_i^2 / \left(\hat{\theta}_i\left\|\hat{s}_{ic}+\hat{s}_{io}\right\| + \varepsilon_{ti}\right) \le \varepsilon_{ti}, \\ &(\hat{s}_{ic}+\hat{s}_{io})^T \tilde{W}_i \sigma(x_{wi}) - \frac{1}{\gamma_{wi}}\mathrm{tr}\left\{\tilde{W}_i^T \mathrm{Proj}_{\hat{W}_i}\left(\gamma_{wi}(\hat{s}_{ic}+\hat{s}_{io})\sigma^T(x_{wi})\right)\right\} \le 0, \\ &\left\|\hat{s}_{ic}+\hat{s}_{io}\right\|\tilde{\theta}_i - \frac{1}{\gamma_{\theta i}}\tilde{\theta}_i \mathrm{Proj}_{\hat{\theta}_i}\left(\gamma_{\theta i}\left\|\hat{s}_{ic}+\hat{s}_{io}\right\|\right) \le 0,\end{aligned} \tag{50}$$

and applying (48) and (50) to (49), one obtains:

$$\dot{V}_i(t) \le -\left(\kappa_{mi} - \kappa_{7i} - \kappa_{8i}\left\|x_i\right\|^2\right)\left\|x_i\right\|^2 + \gamma_i, \tag{51}$$

where $\kappa_{mi} = \min\left\{\kappa_{ji}\right\}_{j=1}^6$ and κ_{ji}, $j = 1, 2, \ldots, 6$ are given by

$$\begin{aligned}\kappa_{1i} &= \kappa_{4i} = \alpha_i \lambda_{\min}(K_{ip}) - 0.5\lambda_{\max}(K_{ip})/\ell - 0.5\beta_i \lambda_{\max}(K_{ip})/\ell, \\ \kappa_{2i} &= \kappa_{5i} = \beta_i \lambda_{\min}(K_{ip}) - 0.5\lambda_{\max}(K_{ip})/\ell - 0.5\beta_i \ell \lambda_{\max}(K_{ip}), \\ \kappa_{3i} &= \lambda_{\min}(K_{ip}+D_i) - \ell\lambda_{\max}(K_{ip}) - 0.5\ell\left(c_{1i}+c_{2i}\right), \\ \kappa_{6i} &= \lambda_{\min}\left(k_{id}M_i(e_i) - K_{ip}\right) - \ell\lambda_{\max}(K_{ip}) - 0.5\ell\left(c_{4i}+c_{5i}\right), \\ \kappa_{7i} &= 0.5\left(c_{1i}/\ell + c_{4i}/\ell + 3c_{3i}\right), \quad \kappa_{8i} = 0.5\left(c_{2i}/\ell + c_{5i}/\ell\right), \\ \gamma_i &= 0.5c_{3i}\left(W_{Mi} + \sqrt{W_{mi}}\right)^2 n_h + 0.5c_3\theta_i^2 + 0.5c_3\theta_{mi}^2 + \varepsilon_{ti}.\end{aligned} \tag{52}$$

The control gains must be chosen such that $\kappa_{ji} > 0$, $j = 1, \ldots, 6$ which result in gains conditions in Theorem 1. If κ_{mi} is chosen such that $\kappa_{mi} > \kappa_{7i} + \kappa_{8i}\left\|x_i\right\|^2$, then, inequality (51) can be stated as $\dot{V}_i(t) \le -\kappa_i\left\|x_i\right\|^2 + \gamma_i$ where κ_i is a positive constant. For the overall formation system, one obtains $\kappa_m > \kappa_7 + \min\left\{\kappa_{8i}\right\}_{i=1}^N \|x\|^2$ where $\kappa_m := \sum_{i=1}^N \kappa_{mi}$, $\kappa_7 := \sum_{i=1}^N \kappa_{7i}$ and $x = [x_1^T, x_2^T, \ldots, x_N^T]^T$. As a result, one gets $\dot{V}(\xi) \le -\kappa_{\min}\|x(t)\|^2 + \gamma$ where $\kappa_{\min} := \min\{\kappa_i\}_{i=1}^N$. This means that $\dot{V}(t)$ is strictly negative outside the compact set $\Omega_x = \left\{x(t) | 0 \le \|x(t)\| \le \sqrt{\gamma/\kappa_{\min}}\right\}$ which implies that $V(t)$ is decreasing outside the set Ω_x. This results in $V(t) \le V(0) \le \lambda_{\vartheta\max}\|\vartheta(0)\|^2$, $\forall t \ge 0$ where the upper bound of $V(t)$ in (45) is used. From this result and (45), one gets $\|x(t)\|^2 \le \left(\lambda_{\vartheta\max}/\lambda_{x\min}\right)\|\vartheta(0)\|^2$, $\forall t \ge 0$. Therefore, a sufficient condition for $\kappa_m > \kappa_7 + \min\left\{\kappa_{8i}\right\}_{i=1}^N \|x\|^2$ is given by $\kappa_m > \kappa_7 + \min\left\{\kappa_{8i}\right\}_{i=1}^N \left(\lambda_{\vartheta\max}/\lambda_{x\min}\right)\|\vartheta(0)\|^2$. This means that the region of attraction R_A in Theorem 1 can be made arbitrarily large to include any initial condition by the proper selection of the control gains. Hence, $\|x(t)\|$ is SGUUB. This result implies that $\xi_{ic}(t), \xi_{io}(t), \varepsilon_i(t), \tilde{q}_i(t), s_{ic}(t), s_{io}(t), \hat{W}_i(t), \tilde{\theta}_i \in L_\infty$, $i = 1, 2, \ldots, N$. The above discussion means that tracking errors and state estimation errors are SGUUB. Therefore, by considering (13)–(18), one concludes that $\dot{\varepsilon}_i(t), \dot{\tilde{q}}_i(t) \in L_\infty$. Finally, considering (7) and (8), the controller (24), and Assumptions 2 and 3, one gets $q_i(t), \hat{q}_i(t), \dot{q}_i(t), v_i(t), \dot{\hat{q}}_i(t), \hat{v}_i(t), \tau_{ai}(t) \in L_\infty$. This completes the proof. □

Remark 2: Since $\det(R_i) = \cos\varphi_i + \sin\varphi_i \tan\gamma_i$ in (8) is non-zero provided that $\tan\varphi_i \tan\gamma_i \neq -1$, a necessary condition to avoid any possible singularity is $|\varphi_i(t)| < \pi/2$ which implies that $|\varphi_{id}| \leq \varphi_{id,\max} < \pi/2$. However, a possible overshoot may violate this condition during the formation construction. Consequently, control gains including K_{ip}, Λ_{i0}, and Λ_{i1} should be adjusted properly to avoid the overshoot.

4. Extension to tractor–trailer mobile robots formation

In this section, the proposed leader–follower formation controller is extended to a group of N TTWMRs. Consider a group of N TTWMRs which are described by (1) where $\eta_i := [x_i, y_i, \theta_{1i}, \theta_{0i}]^T$ represents the position (x_i, y_i) and orientation θ_{1i}, θ_{0i} of the ith tractor and trailer with respect to the earth-fixed frame in Figure 4. The kinematic model of TTWMRs is described by (2) where $s_{1i}(\eta_i) = [\cos\theta_{1i}, \sin\theta_{1i}, (1/d_i)\tan(\theta_{0i} - \theta_{1i}), 0]^T$ and $s_{2i}(\eta_i) = [0, 0, 0, 1]^T$ for the case of $d_{0i} = 0$ and $d_{1i} = d_i$ (on-axle hitching) [25], $v_i(t)$ is the linear velocity of P_{1i} in Figure 4 and $\omega_i(t)$ shows the angular velocity of the tractor subsystem. For a detailed description of the tractor–trailer systems and definitions of their parameters, the readers are referred to [25]. Then, the TTWMR dynamic model is converted to (3) similarly. To develop a second-order leader–follower formation model as in Section 2, posture errors between ith TTWMR and the virtual leader in the earth-fixed frame $\{O_E, X_E, Y_E\}$ are transformed to the body-fixed frame $\{O_{Bi}, X_{Bi}, Y_{Bi}\}$ by the transformation $e_i(t) = T_i(\theta_{1i})(\eta_d - \eta_i)$ where T_i is defined by (4).

The time derivative of this equation yields the following error equation in the body-fixed frame:

$$\begin{bmatrix} \dot{e}_{i1}(t) \\ \dot{e}_{i2}(t) \\ \dot{e}_{i3}(t) \\ \dot{e}_{i4}(t) \end{bmatrix} = \underbrace{\begin{bmatrix} -1 + (e_{i2}/d_i)\tan(\theta_{0i} - \theta_{1i}) & 0 \\ -(e_{i1}/d_i)\tan(\theta_{0i} - \theta_{1i}) & 0 \\ -(1/d_i)\tan(\theta_{0i} - \theta_{1i}) & 0 \\ 0 & -1 \end{bmatrix}}_{J_i} \begin{bmatrix} v_i \\ \omega_i \end{bmatrix} + \underbrace{\begin{bmatrix} \cos e_{i3} & 0 \\ \sin e_{i3} & 0 \\ 1/d_d \tan(\theta_{0d} - \theta_{1d}) & 0 \\ 0 & 1 \end{bmatrix}}_{S_i} \underbrace{\begin{bmatrix} v_d \\ \omega_d \end{bmatrix}}_{v_d}. \quad (53)$$

Then, the virtual range and bearing angle of ith follower are defined as follows:

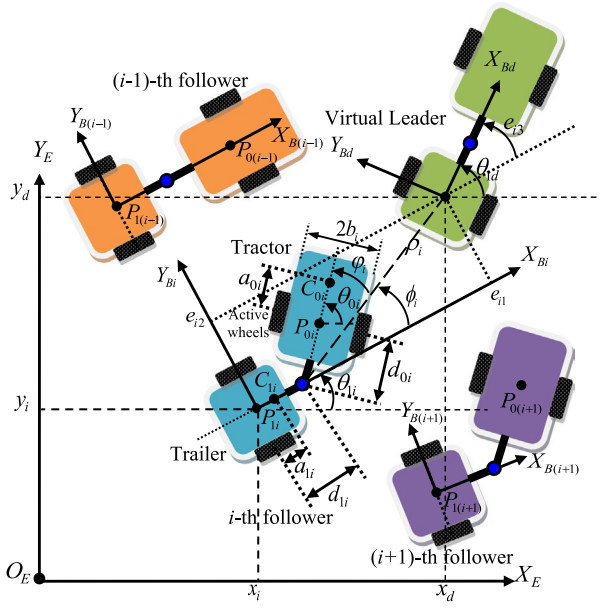

Figure 4. The outline of virtual leader–follower formation control of tractor–trailer systems.

$$q_i(t) = \begin{bmatrix} \rho_i(t) \\ \varphi_i(t) \end{bmatrix} = \begin{bmatrix} \rho_i(t) \\ \phi_i(t) - (\theta_{0i} - \theta_{1i}) \end{bmatrix} = \begin{bmatrix} \sqrt{(e_{i1}(t) - d_{1i})^2 + e_{i2}^2(t)} \\ atan2(e_{i2}(t), e_{i1}(t) - d_{1i}) - (\theta_{0i} - \theta_{1i}) \end{bmatrix}. \quad (54)$$

By differentiating (54) and replacing (53), one obtains

$$\dot{q}_i(t) = \underbrace{\begin{bmatrix} -\cos\phi_i - \sin\phi_i \tan(\theta_{0i} - \theta_{1i}) & 0 \\ (\sin\phi_i - \cos\phi_i \tan(\theta_{0i} - \theta_{1i}))/\rho_i & -1 \end{bmatrix}}_{R_i(\eta,\eta_d)} v_i + \underbrace{\begin{bmatrix} v_d \cos(e_{i3} - \phi_i) \\ v_d \sin(e_{i3} - \phi_i)/\rho_i \end{bmatrix}}_{\delta_i}. \quad (55)$$

Then, one gets the formation model $M_i\ddot{q}_i + C_i\dot{q}_i + D_i\dot{q}_i - \bar{D}_i\dot{q}_i + f_i + \tau_{di}(t) = B_i\tau_{ai}$ similar to Section 2. Finally, theoretical results of Theorem 1 can be applied to the formation control of N TTWMRs. A necessary condition to avoid any possible singularity is given by $|\varphi_{id}| \leq \varphi_{id,\max} < \pi/2$.

5. Numerical simulations

5.1. CLMRs formation

In this section, the effectiveness of the proposed formation controller is evaluated for a group of CLMRs. For this

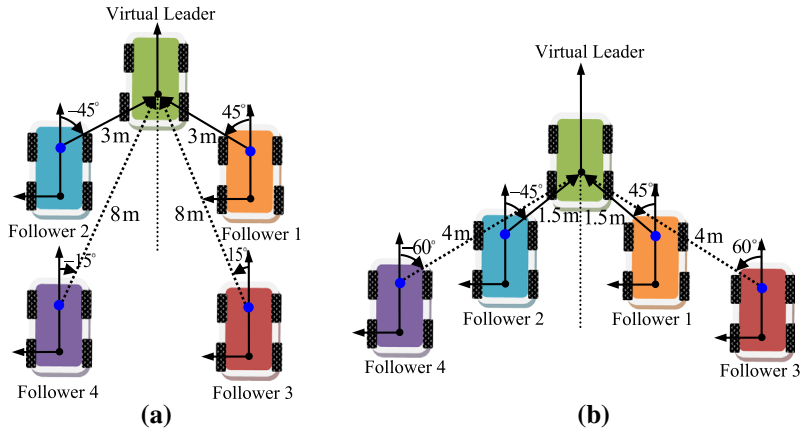

Figure 5. Desired configurations of the leader–follower formation for (a) the linear trajectory and (b) the circular trajectory.

purpose, four identical CLMRs are commanded to follow a virtual leader based on a predefined desired formation. All of simulations are performed in MATLAB software by employing Euler's approximation method with a 20 ms sampling time. Gaussian white noise is appended to posture states using *randn*(●) function to simulate the uncertainty in the localization system. For the purpose of this simulation, the inertia, Coriolis and input transformation matrices are given as follows [24]:

$$M_{1i}(\eta_i) = \begin{bmatrix} m_{ci} & 0 & -m_{ci}l_{ci}\sin\psi_i & 0 \\ 0 & m_{ci} & m_{ci}l_{ci}\cos\psi_i & 0 \\ -m_{ci}l_{ci}\sin\psi_i & m_{ci}l_{ci}\cos\psi_i & I_{ci}+I_{fi} & I_{fi} \\ 0 & 0 & I_{fi} & I_{fi} \end{bmatrix},$$

$$C_{1i}(\eta_i,\dot{\eta}_i)\dot{\eta}_i = \begin{bmatrix} -m_{ci}l_{ci}\dot{\psi}_i^2\cos\psi_i \\ -m_{ci}l_{ci}\dot{\psi}_i^2\sin\psi_i \\ 0 \\ 0 \end{bmatrix}, \quad (56)$$

$$B_{1i}(\eta_i) = \begin{bmatrix} \cos\psi_i & 0 \\ \sin\psi_i & 0 \\ a_i\sin\gamma_i\cos\gamma_i & 0 \\ 0 & 1 \end{bmatrix}.$$

Physical parameters of all CLMRs are given by $r_i = 0.2$ m, $m_{ci} = 30$ kg, $I_{ci} = 5\,\text{kg m}^2$ and $I_{fi} = 10\,\text{kg m}^2$, $a_i = 1.2$ m represents the wheelbase, $l_{ci} = 0.55$ m is the distance between the point O_{Bi} and P_{ci} according to Figure 1 and $D_{1i} = 25I_4$ denotes the matrix of damping coefficients.

In the first simulation, the desired torque and initial posture of the virtual leader is considered as $\tau_{ad} = [8, 0]^T$ and $\eta_d = [2.5, 5.5, 0, 0]^T$, respectively, to generate a linear trajectory. The initial postures of followers are given by $\eta_1 = [-5, 0, 0, 0]^T$, $\eta_2 = [-5, 10, 0, 0]^T$, $\eta_3 = [-5, 15, 0, 0]^T$, and $\eta_4 = [-5, -5, 0, 0]^T$. The controller and observer gains are chosen as $K_{ip} = 10I_2$, $\Lambda_{i0} = 2I_2$, $\Lambda_{i1} = 0.05I_2$, $k_{id} = 10$, $\varepsilon_{ti} = 10$, $\gamma_{\theta i} = 0.5$, and $\theta_{mi} = 10$. Furthermore, a projection-type RBFNN with nine hidden nodes ($n_h = 9$), two output nodes ($n_o = 2$) and the parameters $\gamma_{wi} = 10$, $W_{mi} = 1000$, $\mu_i = [-4, -3, -2, -1, 0, 1, 2, 3, 4]^T$, and $\lambda_i = 10[1, 1, 1, 1, 1, 1, 1, 1, 1]^T$ is used for the control system of all CLMRs. $\hat{W}_i$, $i = 1, \ldots, 4$ are 2×9 matrices whose initial values are set to zero. The control signals are saturated within $|\tau_{aik}| \leq 200$ Nm, $k = 1, 2$ to simulate the input saturation of real actuators. Desired formation vectors are chosen as $q_{1d}(t) = [3, 45°]^T$, $q_{2d}(t) = [3, -45°]^T$, $q_{3d}(t) = [8, 15°]^T$, and $q_{4d}(t) = [8, -15°]^T$ which are illustrated by Figure 5(a). The initial conditions of the observer are selected as $\tilde{q}_i(0) = 0$, $p_{i0} = 0$ and $\dot{\hat{q}}_i(0) = 0$. All controller gains are adjusted based on trial and error method to obtain the best tracking performance. Simulation results including robot trajectories, output tracking errors, control signals, estimated range and bearing angles and estimated velocity errors are shown by Figure 6. It is obvious that all CLMRs successfully track the desired formation of Figure 5(a) without velocity measurements.

In the second simulation, the initial posture of the virtual leader is considered as $\eta_d = [2.5, 5.5, 0, 0.1]^T$ to generate a circular trajectory. Desired formation vectors are chosen as $q_{1d}(t) = [1.5, 45°]^T$, $q_{2d}(t) = [1.5, -45°]^T$, $q_{3d}(t) = [4, 60°]^T$, and $q_{4d}(t) = [4, -60°]^T$. The controller and observer gains are chosen same as the first simulation except that $\gamma_{\theta i} = 0.25$, $\theta_{mi} = 20$, $\gamma_{wi} = 0.1$, and $W_{mi} = 100$. All robots are commanded to construct the desired formation configuration in Figure 5(b). Simulation results including x–y plot of CLMRs formation, range and bearing tracking errors, generated torque signals, velocities estimation errors, and weights and parameters estimates

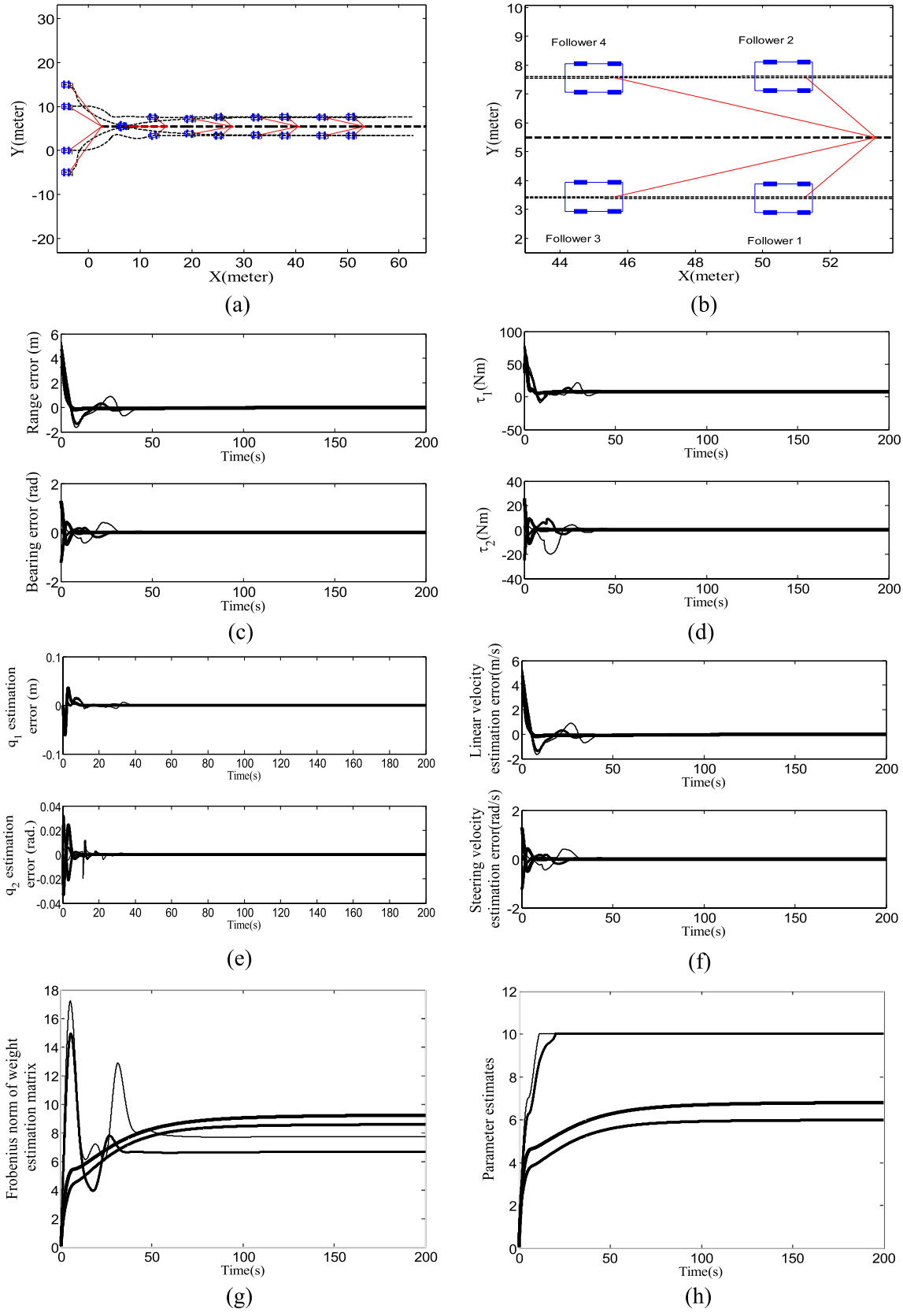

Figure 6. Simulation results for a linear trajectory (a) *x*–*y* plot of CLMRs formation, (b) enlarged view of *x*–*y* plot, (c) range and bearing tracking errors, (d) generated torque signals, (e) *q* estimation errors, (f) velocities estimation errors, (g) Frobenius norm of weight matrix estimation, and (h) parameters estimates.

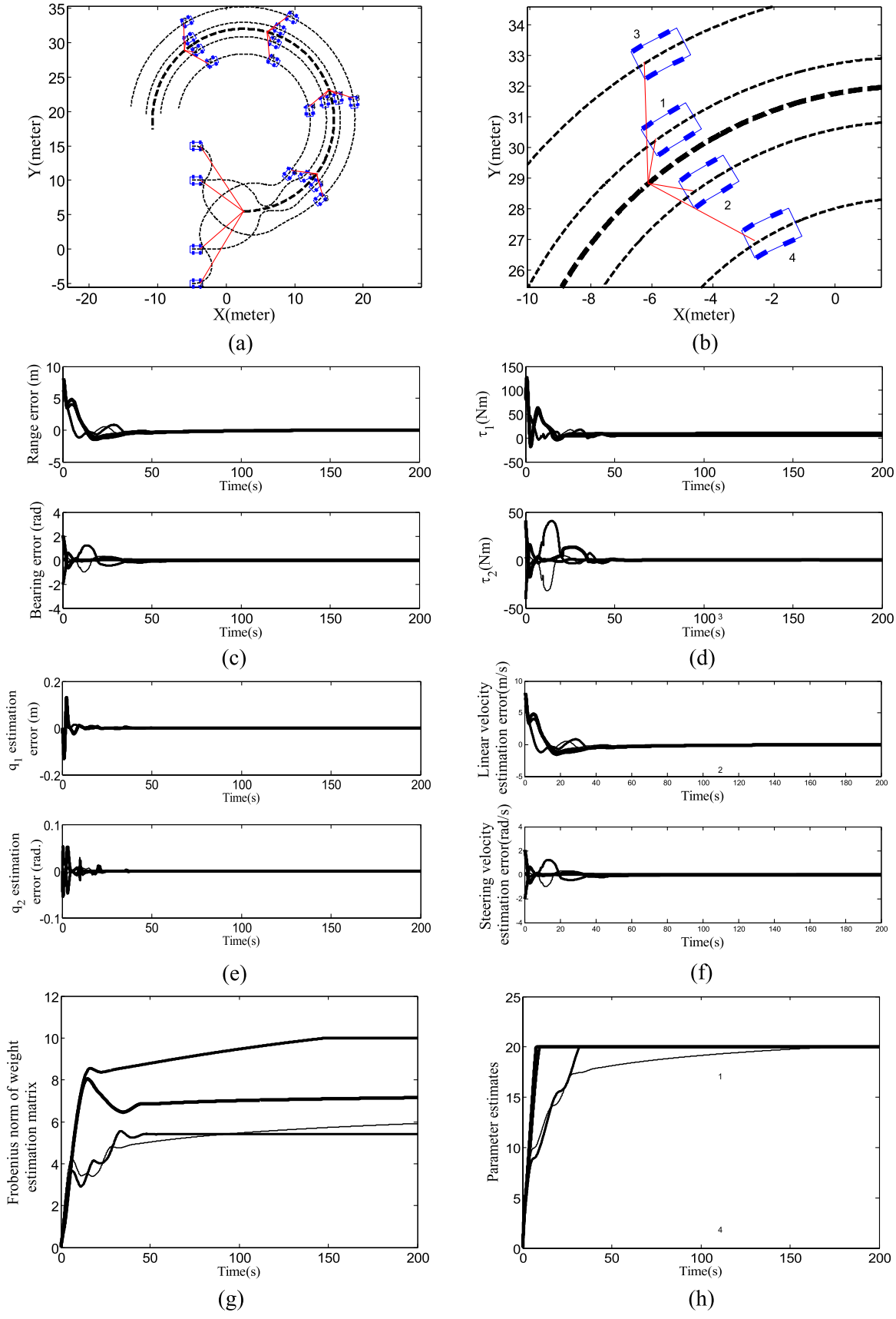

Figure 7. Simulation results for a circular trajectory (a) *x*–*y* plot of CLMRs formation, (b) enlarged view of *x*–*y* plot, (c) range and bearing tracking errors, (d) generated torque signals, (e) *q* estimation errors, (f) velocities estimation errors, (g) Frobenius norm of weight matrix estimation, and (h) parameters estimates.

are illustrated by Figure 7. This figure shows that all of followers successfully track the desired formation in the presence of parametric and non-parametric uncertainties without velocity measurements. Similar to Figure 6, tracking results of Figure 7(c), (e) and (f) confirm that the formation tracking errors, range, bearing angle, and velocity estimation error signals converge to neighborhoods of the origin. Figure 7(d) demonstrates that the proposed controller generates feasible control signals for real implementations. Figure 7(g) and (h) also show that weights and parameters estimates are bounded by predefined constraints via the projection-type update rules (28)–(30). Moreover, simulation results demonstrate that smaller values of ε_{ti} in the controller (24) increase the final tracking accuracy in expense of more chattering in control signals. It should be noted that the user may tune control gains to compromise between the formation tracking performance, robustness, and smoothness of control signals.

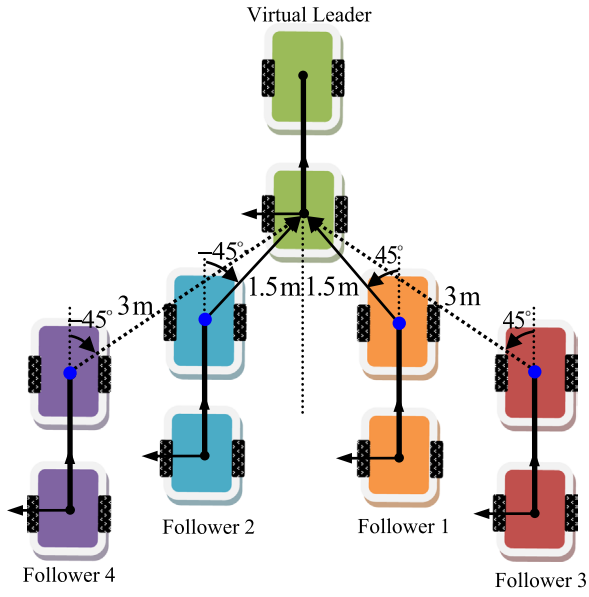

Figure 8. Desired configuration of the leader–follower formation for a team of on-axle TTWMRs.

5.2. TTWMRs formation

The proposed leader–follower formation controller is evaluated for a team of four on-axle TTWMRs in this section. According to [25], dynamic matrices are given by

$$A_i(\eta_i) = \begin{bmatrix} \sin\theta_{0i} & -\cos\theta_{0i} & -d_i\cos(\theta_{0i}-\theta_{1i}) & 0 \\ \sin\theta_{1i} & -\cos\theta_{1i} & 0 & 0 \end{bmatrix}^T,$$

$$M_i(\eta_i) = \begin{bmatrix} M_i & 0 & -L_i\sin\theta_{1i} & -a_{0i}m_{0i}\sin\theta_{0i} \\ 0 & M_i & L_i\cos\theta_{1i} & a_{0i}m_{0i}\cos\theta_{0i} \\ -L_i\sin\theta_{1i} & L_i\cos\theta_{1i} & I_{\theta_{1i}} & a_{0i}d_im_{0i}\cos(\theta_{0i}-\theta_{1i}) \\ -a_{0i}m_{0i}\sin\theta_{0i} & a_{0i}m_{0i}\cos\theta_{0i} & a_{0i}d_im_{0i}\cos(\theta_{0i}-\theta_{1i}) & I_{\theta_{0i}} \end{bmatrix}, \quad (57)$$

$$C_i(\eta_i,\dot\eta_i)\dot\eta_i = \left[C_{jki}\right]_{4\times1}, \quad D_i = diag[d_{m1i}, d_{m2i}, d_{m3i}, d_{m4i}],$$

$$B_i = \frac{1}{r_i}\begin{bmatrix} \cos\theta_{0i} & \sin\theta_{0i} & d_i\sin(\theta_{0i}-\theta_{1i}) & b_i \\ \cos\theta_{0i} & \sin\theta_{0i} & d_i\sin(\theta_{0i}-\theta_{1i}) & -b_i \end{bmatrix}^T,$$

where robot parameters are $M_i = m_{0i} + m_{1i}$, $L_i = a_{1i}m_{1i} + d_im_{0i}$, $I_{\theta_{1i}} = m_{1i}a_{1i}^2 + m_{0i}d_i^2 + I_{1i}$, $I_{\theta_{0i}} = m_{0i}a_{0i}^2 + I_{0i}$, $C_{11i} = -a_{0i}m_{0i}\cos\theta_{0i}\dot\theta_{0i}^2 - L_i\cos\theta_{1i}\dot\theta_{1i}^2$, $C_{21i} = -a_{0i}m_{0i}\sin\theta_{0i}\dot\theta_{0i}^2 - L_i\sin\theta_{1i}\dot\theta_{1i}^2$, $C_{31i} = -a_{0i}d_im_{0i}\dot\theta_{0i}^2\sin(\theta_{0i}-\theta_{1i})$ and $C_{41i} = a_{0i}d_im_{0i}\dot\theta_{1i}^2\sin(\theta_{0i}-\theta_{1i})$ where $m_{0i} = 15\,\text{kg}$ and $m_{1i} = 15\,\text{kg}$ denote the mass of the tractor and trailer, respectively, $I_{0i} = 2\,\text{kg m}^2$ and $I_{1i} = 2\,\text{kg m}^2$ are their moments of inertia about vertical axes, $r_i = 0.15\,\text{m}$ is the radius of tractor wheels, $2b_i = 0.8\,\text{m}$ is the distance between two active wheels of the tractor, $a_{0i} = 0.15\,\text{m}$ and $a_{1i} = 0.05\,\text{m}$ represent distances between center of masses and the midpoint of tractor and trailer wheels, respectively.

Here, it is assumed that $d_i = d_{1i} = 1.5\,\text{m}$ and $d_{0i} = 0$. For a detailed description of tractor–trailer system parameters, the interested readers are referred to [25]. In this simulation, initial postures of followers and the virtual leader are given by $\eta_1 = [0, 2, 0, 30°]^T$, $\eta_2 = [0, -2, 0, -30°]^T$, $\eta_3 = [0, 4, 0, -15°]^T$, $\eta_4 = [0, -4, 0, 15°]^T$, and $\eta_d = [5, 0, 0, 0]^T$. Desired formation vectors are given by $q_{1d}(t) = [1.5, 45°]^T$, $q_{2d}(t) = [1.5, -45°]^T$, $q_{3d}(t) = [3, 45°]^T$, and $q_{4d}(t) = [3, -45°]^T$. Other simulation conditions are same as the previous simulation. The desired torque of the virtual leader is set to $\tau_{ad} = [0.35, 0.5]^T$ and all followers are forced to construct the desired formation of Figure 8. Figure 9 shows that all TTWMRs successfully track the desired formation in the presence of model uncertainties and without velocity measurements.

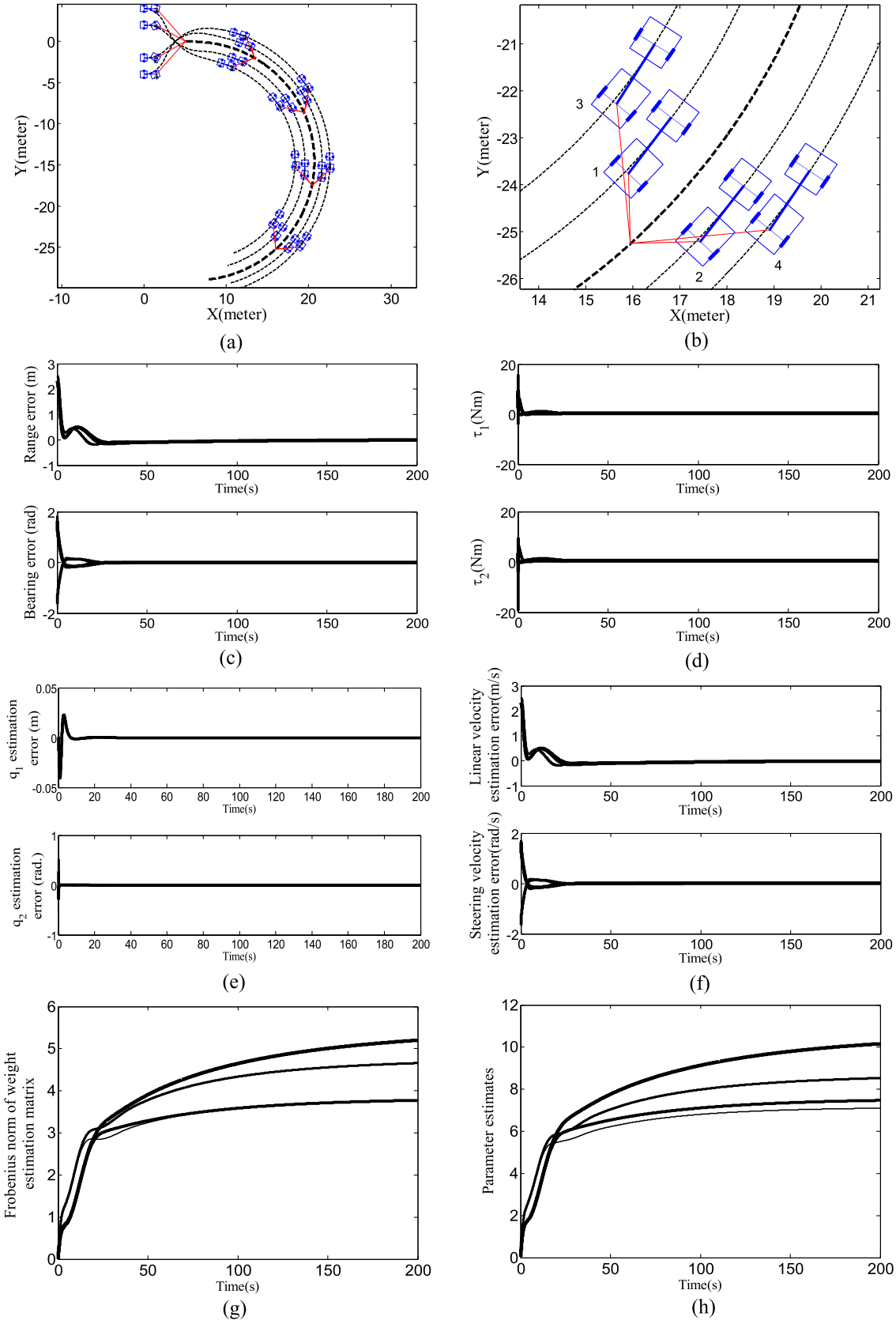

Figure 9. Simulation results for four TTWMRs formation (a) *x*–*y* plot, (b) enlarged view of *x*–*y* plot, (c) range and bearing tracking errors, (d) generated torque signals, (e) *q* estimation errors, (f) velocities estimation errors, (g) Frobenius norm of weight matrix estimation, and (h) parameters estimates.

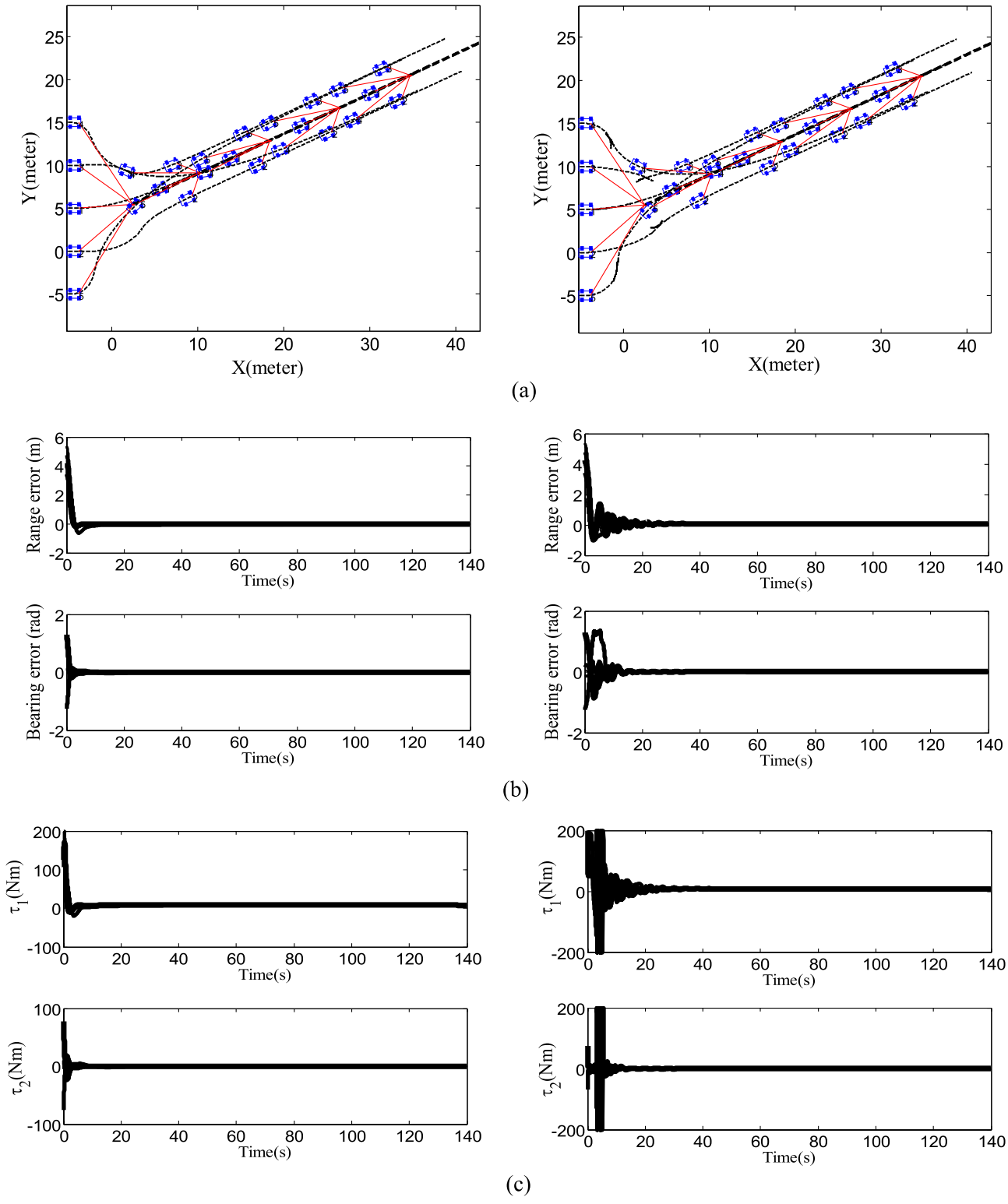

Figure 10. Comparative simulation results for the proposed controller (left column) and neural high-gain observer-based controller in [29] (right-column): (a) *x*–*y* plot, (b) tracking errors, and (c) control signals.

5.3. A comparative simulation study

In this section, a comparative simulation is performed to evaluate the tracking performance of the proposed formation controller in comparison with the following neural OFB formation controller which is designed based on [29] by the backstepping technique:

$$\begin{cases} \alpha_{1i} = R_i^{-1}(e_i, \gamma_d)\left(\dot{q}_{id}(t) - K_{1i} z_{1i} - \delta_i(e_i, \upsilon_d)\right) \\ \tau_{ai}(t) = B_{2i}^{-1}(\eta_i)\left(-R_i^T(e_i, \gamma_d) z_{1i} - K_{2i}\hat{z}_{2i} + \hat{\Theta}_i^T S(\hat{Z}_i)\right), \\ \dot{\hat{\theta}}_{ij} = -\Gamma_{ij}\left(S_j(\hat{Z}_i)\hat{z}_{2ij} + \sigma_{ij}\hat{\theta}_{ij}\right), \\ \hat{z}_{2i} = \hat{v}_i - \alpha_{1i} = R_i^{-1}(e_i, \gamma_d)\left(\dot{\hat{q}} - \delta_i(e_i, \upsilon_d)\right) - \alpha_{1i}, \end{cases} \tag{58}$$

where $z_{1i} = q_i(t) - q_{id}(t)$, $\hat{\Theta}_i := \text{blockdiag}\left[\hat{\theta}_{i1}^T, \hat{\theta}_{i2}^T, \hat{\theta}_{i3}^T\right]$ denotes estimated NN parameters, $S(\hat{Z}_i) = \left[S_1^T(\hat{Z}_i), S_2^T(\hat{Z}_i), S_3^T(\hat{Z}_i)\right]^T$ shows radial basis functions, $\hat{Z}_i = \left[q_i^T, \hat{v}_i^T, \alpha_{1i}^T, \dot{\alpha}_{1i}^T\right]^T$ and $\dot{\hat{q}}_i$ is estimated by the following high-gain observer:

$$\begin{cases} \dot{\hat{q}}_i = \pi_{2i}/\varepsilon_i, \quad i = 1, 2, \ldots, N \\ \varepsilon_i \dot{\pi}_{1i} = \pi_{2i}, \quad \varepsilon_i \dot{\pi}_{2i} = -\gamma_{1i}\pi_{2i} - \pi_{1i} + q_i, \end{cases} \tag{59}$$

where ε_i, $\gamma_{1i} > 0$ and π_{ji}, $j = 1, 2$ represent observer parameters and variables. The design procedure and complete definitions can be found in [29]. In order to provide a fair comparison, control parameters are tuned such that best tracking performances are obtained for both controllers. For this simulation, five CLMRs are considered such that $q_{1d}(t) = [4.5, 0°]^T$, $q_{2d}(t) = [3, 45°]^T$, $q_{3d}(t) = [3, -45°]^T$, $q_{4d}(t) = [8, 15°]^T$, $q_{5d}(t) = [8, -15°]^T$, $\eta_1 = [-5, 5, 0, 0]^T$, $\eta_2 = [-5, 0, 0, 0]^T$, $\eta_3 = [-5, 10, 0, 0]^T$, $\eta_4 = [-5, 15, 0, 0]^T$, $\eta_5 = [-5, -5, 0, 0]^T$, $\eta_d = [2.5, 5.5, 25°, 0]^T$ and other parameters are similar to the first simulation.

Figure 10 shows simulation results. Both controllers successfully construct the desired formation. However, the tracking performance of the proposed controller (Figure 10, left column) is better than the controller (58) and (59) (Figure 10, right column). Other simulations also confirm a better performance of the proposed controller.

6. Conclusion

The OFB PID formation control of a team of CLMRs has been studied in this paper. For this purpose, a second-order leader–follower formation dynamic model has been introduced by transforming posture errors of *i*th follower into virtual range and bearing errors. Then, an observer-based PID formation control scheme has been proposed to make all followers track a virtual leader without velocity measurements. External disturbances, unmodeled dynamics and unknown model parameters have been effectively compensated by neural network and adaptive robust techniques. From a Lyapunov-based stability analysis, it was proved that all signals in the closed-loop formation system are bounded. In addition, the range and bearing tracking and observation errors are SGUUB and converge to a small bound containing the origin. Moreover, the proposed method has been extended to the formation control of *N* TTWMRs. Finally, simulation results have shown that the proposed controller provides a good formation tracking performance and robustness against model uncertainties for real-world applications. The future work is devoted to the experimental evaluation of the proposed formation controller by real robots in order to confirm its effectiveness in practice.

Disclosure statement

No potential conflict of interest was reported by the author.

Funding

This work was supported by the Najafabad Branch, Islamic Azad University [grant number 1509512080049] under the research project 'Coordinated Control of Autonomous Vehicles and Unmanned Cars without Velocity Sensors by Using Adaptive Neural Networks.'

Notes on contributor

Khoshnam Shojaei was born in Esfahan, Iran, on 8 March 1981. He received his BS degree, MS degree, and PhD degree with distinction in electrical engineering from Iran University of Science and Technology (IUST) in 2004, 2007, and 2011, respectively. Currently, he is an assistant professor in Najafabad Branch, Islamic Azad University, Iran. His research areas are the adaptive control of nonlinear systems, control of autonomous robots including land, air and ocean vehicles, and the navigation of mobile robots.

References

[1] Balch T, Arkin RC. Behavior-based formation control for multirobot teams. IEEE Trans Robot Autom. 1998;14(6):926–939.
[2] Fredslund J, Mataric MJ. A general algorithm for robot formations using local sensing and minimal communication. IEEE Trans Robot Autom. 2002;18(5):837–846.
[3] Lewis MA, Tan K-H. High precision formation control of mobile robots using virtual structures. Autonom Robots. 1997;4(4):387–403.
[4] Do KD. Formation tracking control of unicycle-type mobile robots with limited sensing ranges. IEEE Trans Control Syst Technol. 2008;16(3):527–538.
[5] Shao J, Xie G, Wang L. Leader-following formation control of multiple mobile vehicles. IET Control Theory Appl. 2007;1(2):545–552.
[6] Consolini L, Morbidi F, Prattichizzo D, et al. Leader and follower formation control of nonholonomic mobile robots with input constraints. Automatica. 2008;44(5):1343–1349.
[7] Defoort M, Floquet T, Kokosy A, et al. Sliding-mode formation control for cooperative autonomous mobile robots. IEEE Trans Industr Electron. 2008;55(11):3944–3953.
[8] Dierks T, Brenner B, Jagannathan S. Neural network-based optimal control of mobile robot formations with reduced information exchange. IEEE Trans Control Syst Technol. 2013;21(4):1407–1415.

[9] Peng Z, Wen G, Rahmani A, et al. Leader-follower formation control of nonholonomic mobile robots based on a bioinspired neurodynamic based approach. Robot Autonom Syst. 2013;61(9):988–996.
[10] Chen X, Jia Y. Adaptive leader-follower formation control of non-holonomic mobile robots using active vision. IET Control Theory Appl. 2015;9(8):1302–1311.
[11] Cai X, de Queiroz M. Adaptive rigidity-based formation control for multirobotic vehicles with dynamics. IEEE Trans Control Syst Technol. 2015;23(1):389–396.
[12] Yoo SJ, Kim T-H. Distributed formation tracking of networked mobile robots under unknown slippage effects. Automatica. 2015;54:100–106.
[13] Sun T, Liu F, Pei H, et al. Observer-based adaptive leader-following formation control for non-holonomic mobile robots. IET Control Theory Appl. 2012;6(18):2835–2841.
[14] Do KD. Output-feedback formation tracking control of unicycle-type mobile robots with limited sensing ranges. Robot Autonom Syst. 2009;57(1):34–47.
[15] Park BS, Park J-B, Choi YH. Adaptive formation control of electrically driven nonholonomic mobile robots with limited information. IEEE Trans Syst Man Cybern B Cybern. 2011;41(4):1061–1075.
[16] Dierks T, Jagannathan S. Neural network output feedback control of robot formations. IEEE Trans Syst Man Cybern B Cybern. 2010;40(2):383–399.
[17] Gil-Pinto A, Fraisse P, Zapata R. Decentralized strategy for car-like robot formation. In: Proceedings of IEEE/RSJ International Conference on Intelligent Robots and Systems; San Diego, CA; 2007. p. 4176–4181.
[18] Panimadai Ramaswamy SA, Balakrishnan SN. Formation control of car-like mobile robots: a Lyapunov function based approach. In: American Control Conference; Seattle, WA; 2008. p. 657–662.
[19] Sadowska A, Huijberts H. Formation control design for car-like nonholonomic robots using the backstepping approach. In: European Control Conference; Zurich, Switzerland; 2013. p. 1274–1279.
[20] Shen D, Sun W, Sun Z. Adaptive PID formation control of nonholonomic robots without leader's velocity information. ISA Trans. 2014;53:474–480.
[21] Berghuis H, Nijmeijer H. A passivity approach to controller-observer design for robots. IEEE Trans Robot Autom. 1993;9(6):740–754.
[22] Shojaei K, Shahri AM. Output feedback tracking control of uncertain non-holonomic wheeled mobile robots: a dynamic surface control approach. IET Control Theory Appl. 2012;6(2):216–228.
[23] Shojaei K. Neural adaptive robust output feedback control of wheeled mobile robots with saturating actuators. Int J Adapt Control Signal Process. 2015;29:855–876.
[24] Chiu C-S, Lian K-Y. Hybrid fuzzy model-based control of nonnholonomic systems: a unified viewpoint. IEEE Trans Fuzzy Syst. 2008;16(1):85–96.
[25] Keymasi Khalaji A, Moosavian SAA. Robust adaptive controller for a tractor-trailer mobile robot. IEEE/ASME Trans Mechatron. 2014;19(3):943–953.
[26] Lewis FL, Dawson DM, Abdallah CT. Robot manipulator control theory and practice. 2nd ed. Revised and Expanded. New York (NY): Marcel Dekker; 2004.
[27] Polycarpou MM. Stable adaptive neural control scheme for nonlinear systems. IEEE Trans Autom Control. 1996;41(3):447–451.
[28] Ioannou PA, Sun J. Robust adaptive control. Englewood Cliffs (NJ): Prentice-Hall; 1996.
[29] Tee KP, Ge SS. Control of fully actuated ocean surface vessels using a class of feedforward approximators. IEEE Trans Control Syst Technol. 2006;14(4):750–756.